Unusual manganese enrichment in the Mesoarchean Mozaan Group, Pongola Supergroup, South Africa

Unusual manganese enrichment in the Mesoarchean Mozaan Group, Pongola Supergroup, South Africa

Frantz Ossa Ossa [a,*], Axel Hofmann [a], Olivier Vidal [b], Jan D. Kramers [a], Georgy Belyanin [a], Barbara Cavalazzi [a,c]

[a] Department of Geology, University of Johannesburg, Auckland Park 2006, Johannesburg, South Africa
[b] LGCA, UMR 5025, Université Joseph Fourier, 1381 rue de la Piscine, BP 53, F-38041 Grenoble Cedex 09, France
[c] Dipartimento di Scienze Biologiche, Geologiche e Ambientali, Università di Bologna, Via Zamboni 67, 40126 Bologna, Italy

ARTICLE INFO

Keywords:
Manganese deposit
Archean
BIF
$^{40}Ar/^{39}Ar$ dating
Mozaan Group
Pongola Supergroup

ABSTRACT

An unusual sediment hosted manganese deposit is described from the Mesoarchean Mozaan Group, Pongola Supergroup, South Africa. MnO contents up to 15 wt.% were observed in marine clastic and chemical sedimentary rocks. Mn enrichment is interpreted to have resulted from the hydrothermal alteration of manganiferous shale and BIF parent rocks, the primary MnO contents of which are as high as 8.5 wt.%. A detailed mineralogical and petrographic study shows that these parent rocks are characterized by manganoan siderite, ferroan rhodochrosite and other Mn–Fe rich mineral phases, such as kutnohorite and Fe–Mn chlorite. Their hypogene alteration gave rise to a diversification of mineral assemblages where ferroan tephroite, calcian rhodochrosite, rhodochrosite, pyrochroite, pyrophanite, cronstedtite, manganoan Fe rich chlorite and manganoan phlogopite partially or totally replaced the previous mineral assemblage. Thermodynamic modeling performed on chlorite phases associated with the described mineral assemblages illustrates a decrease of average crystallization temperatures from ca. 310 °C during early metamorphic stages to ca. 250 °C during a hydrothermal stage. Mineral transformation processes were thus related to retrograde metamorphism and/or hydrothermal alteration post dating metamorphism and gave rise to progressive Mn enrichment from unaltered parent to altered rocks. The timing of hypogene alteration was constrained by $^{40}Ar/^{39}Ar$ dating to between about 1500 and 1100 Ma ago, reflecting tectonic processes associated with the Namaqua Natal orogeny along the southern Kaapvaal Craton margin. Manganiferous shale and BIF of the Mozaan Group may represent the oldest known examples of primary sedimentary Mn deposition, related to oxidation of dissolved Mn(II) by free oxygen in a shallow marine environment. Oxygenic photosynthesis would have acted as a first order control during Mn precipitation. This hypothesis opens a new perspective for better constraining secular evolution of sediment hosted mineral deposits linked to oxygen levels in the atmosphere–hydrosphere system during the Archean Eon.

1. Introduction

Manganese deposits of diverse genetic types (e.g., hydrothermal, sedimentary, continental weathering, deep sea nodule) occur in the geological record from Archean to Recent (Beukes and Gutzmer, 1996; Ingri, 1985; Gauthier Lafaye and Weber, 2003; Pack et al., 2000; Roy, 2000, 2006). Manganese minerals associated with iron formations commonly precipitated from seawater where Mn and Fe were derived from hydrothermal venting associated with submarine volcanic activity. Large scale precipitation was driven by changes in the redox state of the oceans (Anbar and Holland, 1992; Gauthier Lafaye and Weber, 2003; Roy, 2000, 2006; Tsikos et al., 2010). Manganese metallogenesis studies have revealed that the most important Mn reserves are associated with Paleoproterozoic sedimentary rocks. The evolution of the O_2 content in the atmosphere–hydrosphere system is considered responsible for the deposition of manganese during this era (Anbar and Holland, 1992; Bekker et al., 2004; Gauthier Lafaye and Weber, 2003; Roy, 2000, 2006; Tsikos et al., 2010). Although Fe rich mineral phases are the dominant components of banded iron formations (BIFs), most of which were deposited during the Archean Eon (Canfield, 2005; Holland, 2005; Isley and Abbott, 1999), almost

* Corresponding author at: Department of Geology, University of Johannesburg, APK Campus-C1 Lab, PO Box 524 Auckland Park 2006, Johannesburg, South Africa. Tel.: +27 115 59 47 15; fax: +27 115 59 47 02.

E-mail address: frantz.ossaossa@gmail.com (F. Ossa Ossa).

all economically exploitable Mn deposits postdate the Great Oxidation Event (GOE) that represents the rise of oxygen in Earth's atmosphere ca. 2.3 billion years ago (Bekker et al., 2004). The 2.2 2.3 billion years old Giant Kalahari Manganese Field in South Africa and the ca. 2.1 billion years old Francevillian Mn ore deposits in Gabon are the largest exploited Precambrian Mn deposits, and formed after the GOE (Bekker et al., 2004; Beukes and Gutzmer, 1996; Gauthier Lafaye and Weber, 2003). However, rare sedimentary manganese ± iron ore deposits are known from successions older than the GOE (Roy, 2000, 2006), possibly indicating fluctua tions in the evolution of atmospheric oxygen levels in deep time.

Archean Mn rich ore deposits are rare, being mined specifically in late Archean greenstone terrains of India and Brazil (Roy, 2000, 2006). In these settings, Mn and Fe are thought to have been released from high temperature hydrothermal solutions and stored initially in anoxic seawater in the dissolved state (Holland, 2002; Roy, 2000, 2006). As the precipitation of Mn in ancient sea water is thought to be redox driven, it is likely that the substantial fixation of CO_2 in large scale carbonate platforms during the late Archean (Beukes and Klein, 1990; Beukes et al., 1990) led to a reduction in atmospheric pCO_2 and, associated with the prolifera tion of stromatolites, a moderate increase in pO_2 in seawater to form restricted oxygenated domains (oxygen oases; Kasting, 1993) in basin margin photic zones (Roy, 2000, 2006). Therefore, late Archean Mn deposition could have been related to those local ized photosynthetic oxygenic domains in shallow marine environ ments (Roy, 2000, 2006).

The Mesoarchean Pongola Supergroup, deposited on the south eastern margin of the Kaapvaal Craton in South Africa, is known to contain shallow marine, epicontinental BIFs (Beukes and Cairncross, 1991) that are locally enriched in Mn (Alexander et al., 2008; Beukes, 1973; Nhleko, 2003), the patchy surface enrichments of which give rise to high grade, but non economical Mn ores in some areas such as Bellevue in northern KwaZulu Natal (De Villiers, 1960).

Considering the major role of redox conditions and related O_2 levels in seawater, we report on unusually high manganese contents of marine BIF and ferruginous shale of the c. 2.95 Ga old Sinqeni and Ntombe formations of the lower Mozaan Group, Pongola Supergroup. With the aid of mineralogical, petrological and chemical investigations, we aim to understand the nature and the origin of unusually high Mn contents within the Mozaan Group and show for the first time that initial Mn concentration was associated with primary sedimentary processes. The variation of Mn contents, mineral paragenesis and processes of Mn enrichment are used to illus trate that the Mozaan Group is host to an exceptional example of a Mesoarchean manganese iron deposits with possibly implication of atmospheric oxygen levels half a billion years before the GOE.

2. Geological setting

The Pongola Supergroup is a Mesoarchean volcano sedimentary sequence deposited ca. 2.98 2.85 Ga on the southeastern margin of the Kaapvaal Craton, South Africa (Gutzmer et al., 1999; Hegner et al., 1994). It crops out in northern KwaZulu Natal, Mpu malanga and Swaziland (Fig. 1) and may be partially correlated with the Witwatersrand Supergroup (Beukes and Cairncross, 1991). The Pongola Supergroup includes two major stratigraphic units: (1) the volcano sedimentary Nsuze Group in the lower part, and (2) the unconformably overlying sedimentary Mozaan Group that is characterized by marine sandstone, shale, and minor BIF (Beukes and Cairncross, 1991; Hicks and Hofmann, 2012). The rocks of the Pongola Supergroup are weakly metamorphosed to lower greenschist facies grade (Burke et al., 1985; Elworthy et al., 2000), except for some areas in Swaziland that record high grade metamorphism (Hofmann et al., 2015). The studied section crops out in the White Mfolozi Inlier (Matthews, 1967), where the Mozaan Group is only represented by its lowermost part, region ally known as the Sinqeni and Ntombe formations (Figs. 1 and 2). The Sinqeni Formation is represented by two sandstone units separated by a succession of ferruginous shale and BIF. The lower sandstone includes (1) the laterally discontinuous Denny Dalton Member of braided alluvial plain conglomerates and pebbly sand stones and (2) the shallow marine, through cross bedded quartz arenites of the Dipka Member (Hicks and Hofmann, 2012). The upper part of this unit is marked by a transgressive ravinement surface, followed by shale and BIF of the Vlakhoek Member, illustrating predominantly sub storm wave base deposition on a clastic sediment starved shelf (Hicks and Hofmann, 2012). The upper sandstone unit, referred to as the Kwaaiman Member, overlies shale along an erosive contact related to sea level fall (Hicks and Hofmann, 2012). The sandstones show symmetrical and interference ripple bedforms, mud cracked mud drapes, flaser bedding and a multitude of microbially induced sedimentary structures (Noffke et al., 2008; Hicks and Hofmann, 2012). A decrease in sedimentary structures indicative of periodic exposure upsection sug gests deposition in an intertidal environment gradually deepening to a shallow subtidal environment. In general, deposition of the Sinqeni Formation was controlled by (eustatic?) sea level changes. Sandstones illustrate deposition in a tide influenced, shallow marine environment under a micro to mesotidal range (Von Brunn and Hobday, 1976; Beukes and Cairncross, 1991; Hicks and Hofmann, 2012; Noffke et al., 2008).

The Ntombe Formation is made up predominantly of ferruginous and non ferruginous shales with minor siltstones and sand stones (Gold, 2006). Sedimentary structures and microbial mat fabrics record a variation between shallow marine, storm dominated shelf and tide influenced environments (Noffke et al., 2003). Except for minor alteration along the contact, there is no visible impact on host rock texture, color or composition caused by the intrusion.

3. Analytical methods

3.1. Sampling

Chemical, petrographic and mineralogical analyses were done on 30 drill core samples of carbonate rich BIF, shale, siltstone and sandstone from the Vlakhoek Member and the Ntombe Formation of the Mozaan Group (Fig. 2), using analytical facilities at Department of Geology and Spectrum Center, University of Johan nesburg. Studied samples were obtained from a core (TSB07 26) drilled close to Denny Dalton Mine (28°16′6.20″S, 031°13′24.33″ E) in the White Mfolozi Inlier (Figs. 1 and 2). All samples are unaffected by recent weathering.

3.2. Petrographic and mineralogical/geochemical characterization

Petrographic analyses were performed on polished thin sections by using an OLYMPUS BX51 polarizing optical microscope equipped with an OLYMPUS DP72 camera. Carbon coated polished thin sections where analyzed using a TESCAN VEGA 3 scanning electron microscope (SEM) at Spectrum. The SEM is equipped with an electron back scattering detector and an energy dispersive spectrometer (EDS). The operating conditions were 20 keV accelerating voltage for both imaging and elemental analyses. Quantitative spot analyses of mineral phases were obtained on carbon coated polished thin sections using a four spectrometer equipped Cameca SX 100 electron probe microanalyzer (EPMA). Operating conditions were 15 keV accelerating voltage, 6 nA beam current,

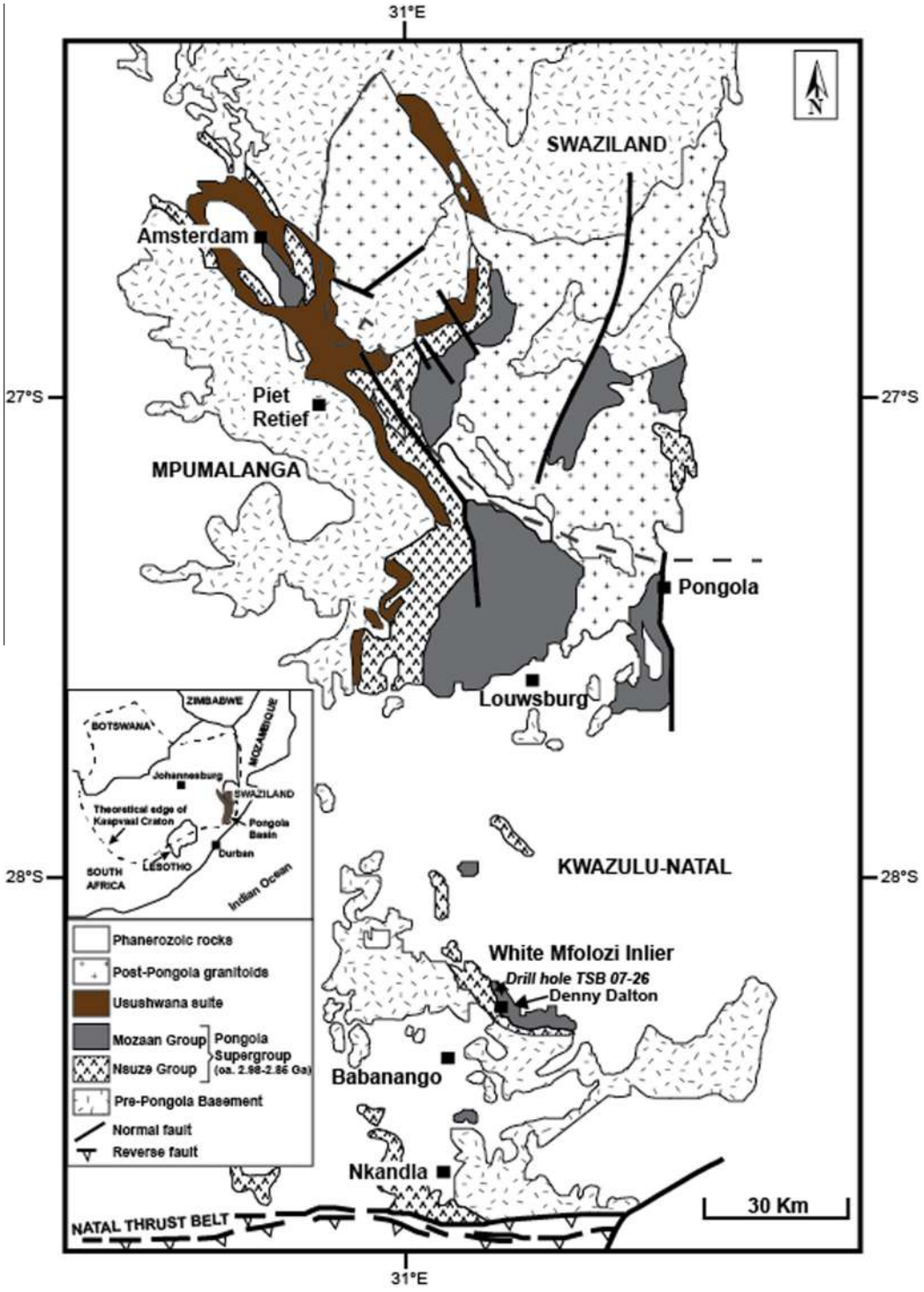

Fig. 1. Geological map of the Pongola Supergroup (modified after Burke et al., 1985).

20 μm spot size for analyses on carbonates, and of 15 keV, 20 nA and 20 μm for oxides and silicates. Almandine (Al), diopside (Si), hematite (Fe), periclase (Mg), $SrSO_4$ (Sr), calcite (Ca), rhodonite (Mn), orthoclase (K), $BaSO_4$ (Ba), TiO (Ti), CrO (Cr), NaCl (Na) and ZnS (Zn) were used as standards. Mineral characterization was completed by XRD and Raman spectroscopy (see Text SI, Figs. S1 3). Powdered samples were analyzed for major elements by X ray fluorescence spectroscopy. Analysis was carried out on fusion beads, using a PANalytical MagiX Pro PW2540 spectrometer. Loss on Ignition (LOI) was determined after heating the samples to 950° C in a furnace for 30 min.

3.3. $^{40}Ar/^{39}Ar$ dating of K rich clay fraction

Aliquots of c. 1 mg of pure illite from the <2 μm fraction, separated from hydrothermally altered samples of the Sinqeni and Ntombe formations, were irradiated at NTP radioisotopes' SAFARI1 nuclear reactor at Pelindaba, South Africa, for 20 h (position B2 W)

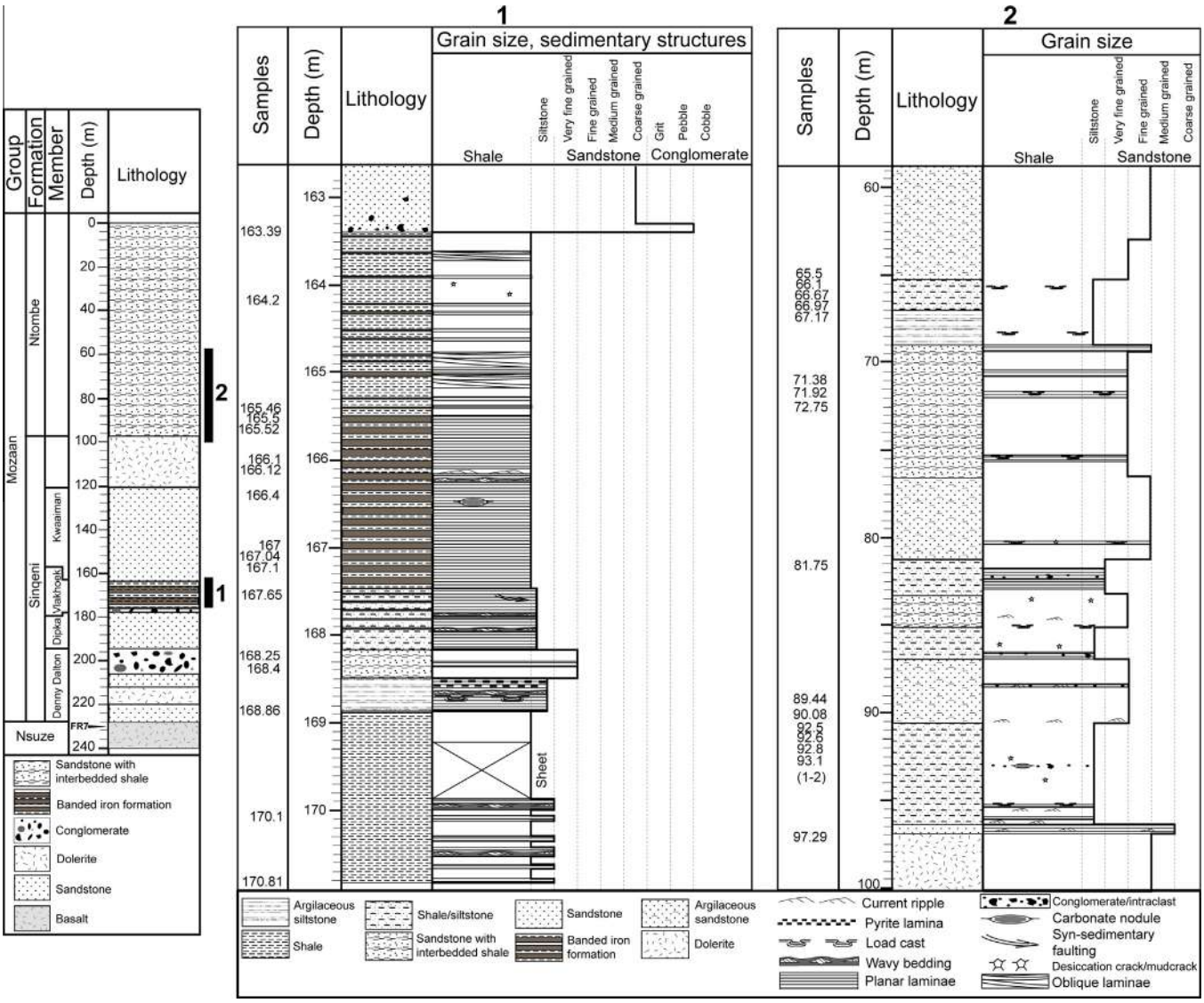

Fig. 2. Stratigraphic column of drill core TSB07-26 of the lower Mozaan Group and details of the studied successions of the Sinqeni Formation (1) and Ntombe Formation (2).

with the reactor running at 20 MW. These were analyzed by stepwise heating, using a defocused beam from a continuous Nd YAG 1064 nm laser and the MAP 215 50 noble gas mass spectrometer at Spectrum. A Johnston focused flow electron multiplier, operated in analog mode, as well as a Faraday collector were used. The amphibole standards McClure Mountains and Hb3GR as well as Fish Canyon Sanidine were used as monitors. All yield the same J values within analytical error. Measurement control and data reduction was done using an in house software suite that includes full error propagation by Monte Carlo procedures.

4. Results

4.1. Sample description and major element distribution

The Vlakhoek Member is represented, from base to top, by a 12 m thick succession of dark grey shale, BIF and dark to light green ferruginous shale (Fig. 2; 3A). This succession is overlain by intertidal to shallow subtidal sandstone of the Kwaaiman Member showing abundant wave ripples (Fig. 3B) as well as early diagenetic carbonate concretions (Fig. 3C). The lower shale of the Vlakhoek Member is 8 m thick and characterized by planar laminated mudstone interbedded with silt rich layers locally showing ripple lamination. BIF is 1.9 m thick and consists of 1 5 cm thick dark grey and red bands of iron oxide, interbedded with carbonate and silica rich bands (e.g. samples 166.4, 165.5 in Fig. 3). The gradation from shale to BIF shows overall deepening of the environment from a marginal marine to a shallow outer shelf environment of an epicontinental sea starved of siliciclastic input during transgression (Hicks and Hofmann, 2012; Planavsky et al., 2014). The upper ferruginous shale is 2.1 m thick and consists of 1 15 cm thick mudstone interbedded with 1 5 cm silt and carbonate rich layers (e.g. sample 165.2 in Fig. 3). Sedimentary structures of the latter succession are predominantly characterized by planar lamination (e.g. sample 165.2 in Fig. 3).

A process of alteration has affected the succession at irregular intervals. Altered rocks have fissure and fracture networks associated with secondary Mn rich phases (e.g. sample 165.5 and 3D in Fig. 3). Alteration halos may extend up to few centimeters away from the fissures. For both BIF and upper shale facies of a total thickness of 4 m, the average MnO content is 7.75 wt.%. MnO content may be as high as 8.5 wt.% in the unaltered rocks, and as high as 11.3 wt.% in the altered rocks (Table 1). BIF samples are characterized by SiO_2 contents ranging from 10 to 36 wt.%, and Fe_2O_3 from 38 to 53 wt.% (Fig. 2, Table 1). The Fe_2O_3 content conforms well with both Algoma and Superior type iron formations,

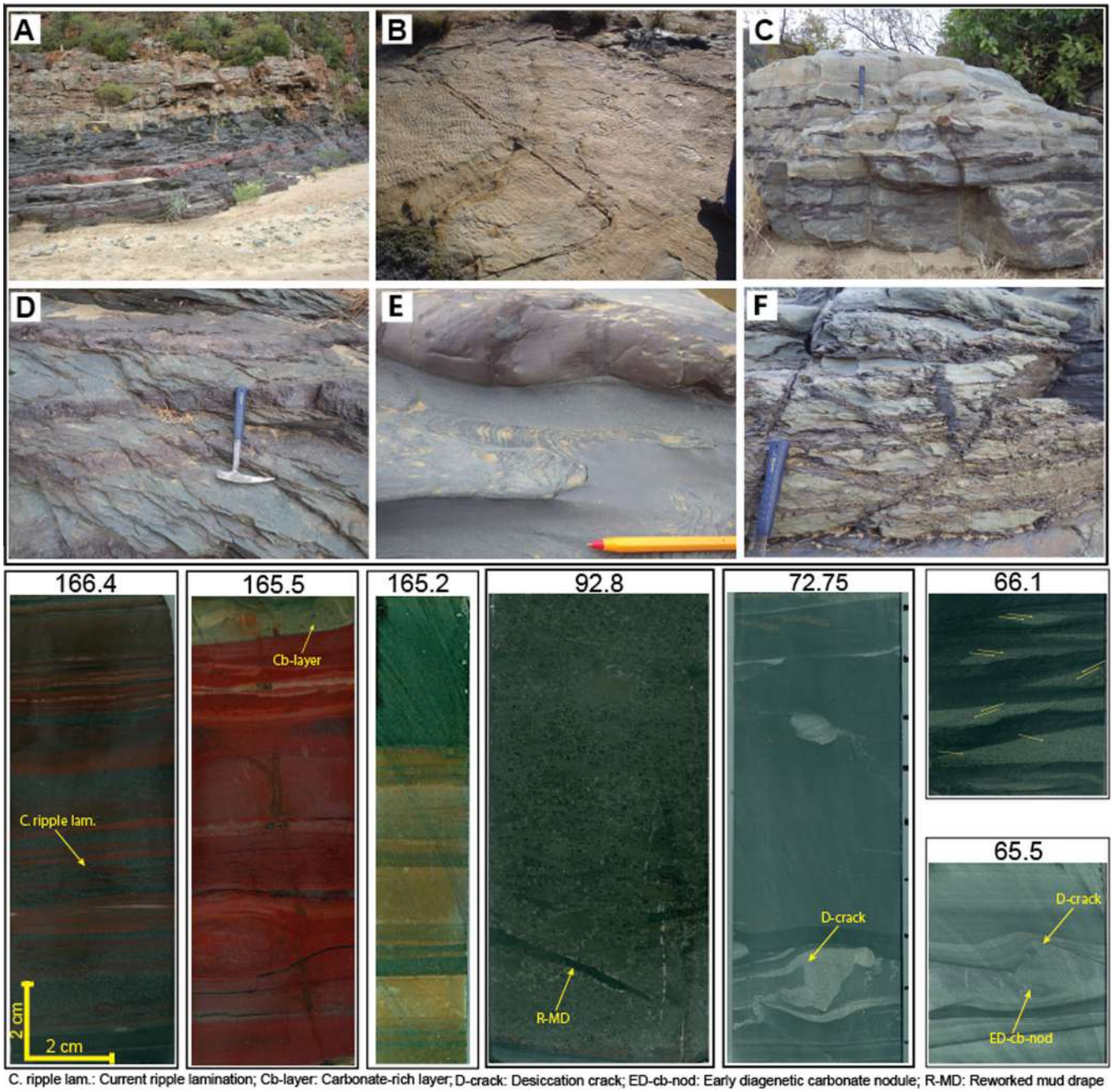

Fig. 3. Photographs of outcrops and drill core showing Mn- and Fe-rich facies of the studied sections. Sample numbers refer to depth (in meters) in the drill core. (A) BIF and ferruginous shale of the Vlakhoek Member erosively overlain by sandstone of the Kwaaiman Member. (B) Pavement of Kwaaiman Member sandstone with wave ripple bedforms. (C) Sandstone with tabular to lensoidal carbonate concretions. (D) Shale showing Mn-carbonate-rich planar beds deformed by foliation dipping to the right of the image. (E) Shale with lenticular carbonate-rich bed. (F) Shale with fractures with alteration halos. A foliation is present dipping at a moderate angle to the right. Sample 166.4: BIF with planar, wavy, and current ripple lamination. Sample 165.5: Thinly bedded jaspilitic BIF associated with carbonate-rich bed. Sample 165.2: Planar laminated green shale with carbonate-rich interbeds. Sample 92.8: Argillaceous sandstone with mudstone intraclasts representing a reworked Mn-rich mud-drape. Samples 72.75-66.1-65.5: Thinly bedded shale with discontinuous beds of fine-grained sandstone showing lenticular bedding (sample 66.1), desiccation cracks (samples 72.75 and 66.1), and early diagenetic carbonate concretion (sample 65.5). (Cb-layer: carbonate-rich layer; D-crack: desiccation crack; R-MD: reworked mud-drape; ED-cb-nod: early diagenetic carbonate nodule).

whereas the MnO content is much higher than the average values found in these types of IFs, and the SiO_2 content appears somewhat lower (Gutzmer et al., 2008). Except for a few clastic mud rich interbeds and the overlying ferruginous shale where the Al_2O_3 con tent is as high as 12.2 wt.%, the Al_2O_3 content mostly ranges from 0.5 to 4 wt.% (Table 1), which is higher than in both Algoma and Superior type deposits but lower than the average of mudrocks of the Mozaan Group (Wronkiewicz and Condie, 1989). However, the shale below the BIF has relatively low MnO and Fe_2O_3 contents of up to 0.7 and 10 wt.%, respectively (Fig. 2, Table 1). SiO_2 contents are up to 56.2 wt.%, with Al_2O_3 reaching 24.6 wt.% (Table 1), which is close to the average of shale in the Mozaan Group (Wronkiewicz and Condie, 1989). In BIF and upper shale, MnO and Fe_2O_3 show a co variation with LOI, with correlation coefficients (R^2) of 0.94 and 0.89, respectively (Fig. 4). Correlation is weaker for LOI vs CaO and MgO (R^2 = 0.52 and 0.72, respectively). This illustrates that both

Table 1
Chemical composition (major elements) of different type of facies in the Sinqeni Formation.

Sample N°	164.2	165.5	165.52	166.1	166.12	166.4	167	167.04	167.1	167.65	168.25	168.4	170.1	171.8	178.4
Host rock	1NA	2NA	2NA	3NA	3NA	3NA	3NA	3A	3A	3NA	3A	3A	1NA	1NA	4NA
SiO_2	30.28	67.52	59.28	23.86	23.52	21.53	25.38	31.43	25.72	24.15	14.95	14.17	54.59	56.23	68.36
Al_2O_3	8.61	0.05	0.42	2.10	3.88	2.44	2.68	1.33	2.08	0.78	2.17	0.59	24.59	22.01	14.61
Fe_2O_3	29.13	18.78	16.42	40.47	39.70	38.51	39.09	39.79	44.18	42.10	41.32	46.04	7.34	9.96	9.43
MnO	8.04	3.27	6.23	7.12	7.18	6.94	7.16	8.50	7.96	8.53	11.28	10.86	0.47	0.68	<dl
MgO	3.66	1.86	4.09	4.79	4.49	4.51	4.52	0.00	4.00	3.98	6.85	5.99	1.85	1.25	<dl
CaO	0.57	0.20	0.57	2.39	2.27	3.67	1.23	0.94	1.06	0.56	0.75	0.66	0.07	<dl	<dl
Na_2O	<dl	<dl	<dl	1.11	1.24	1.99	<dl	<dl	<dl	<dl	<dl	<dl	1.57	1.20	0.16
K_2O	<dl	<dl	<dl	<dl	0.05	<dl	<dl	<dl	<dl	<dl	<dl	<dl	4.25	2.65	0.49
TiO_2	0.32	<dl	<dl	<dl	0.10	0.06	0.11	<dl	0.05	<dl	<dl	<dl	0.84	0.85	0.24
Cr_2O_3	<dl	<dl	<dl	<dl	<dl	<dl	<dl	<dl	<dl	<dl	<dl	<dl	<dl	0.05	0.11
P_2O_5	0.05	<dl	<dl	0.11	<dl	<dl	0.09	0.14	0.26	0.08	0.15	0.05	0.08	0.05	<dl
LOI*	19.15	6.82	12.74	17.03	16.64	19.63	19.13	17.60	14.05	19.20	22.01	21.33	4.24	4.39	6.39
Total	99.82	98.53	99.78	99.03	99.10	99.30	99.42	99.72	99.36	99.38	99.48	99.71	99.93	99.36	99.89
MnO/(MnO + Fe_2O_3)	0.22	0.15	0.28	0.15	0.15	0.15	0.15	0.18	0.15	0.17	0.21	0.19	0.06	0.06	0.00

Major element concentrations obtained by XRF in wt.%. 1NA = unaltered carbonate-rich shale; 2NA = unaltered jasper; 3NA = unaltered banded iron formation (BIF); 3A = altered BIF; 4NA = unaltered argillaceous sandstone/siltstone. * = LOI (lost on ignition) after 30 min at 930 °C in air; <dl = concentration below the detection limit of 0.05 wt.%.

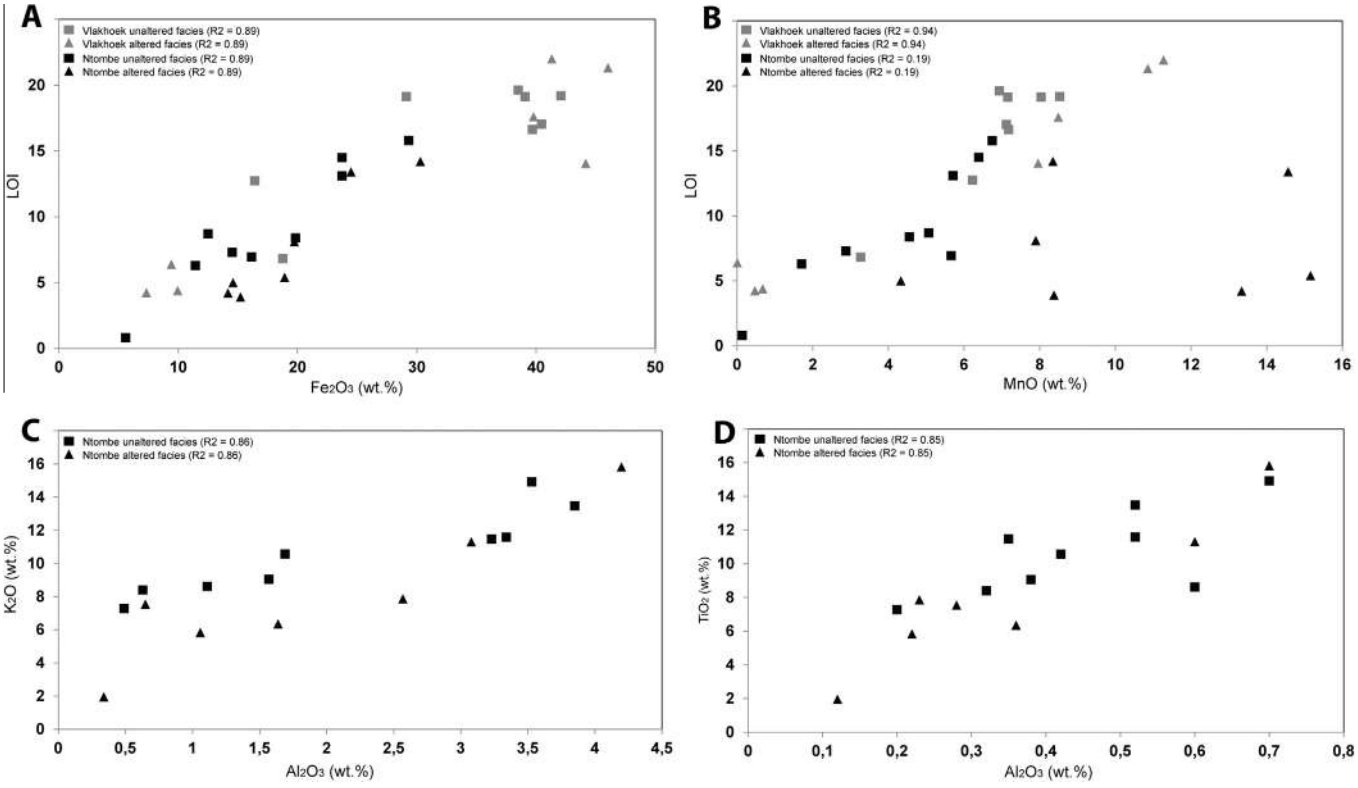

Fig. 4. Co-variation between some major elements and loss on ignition (LOI). Diagrams of (A) LOI *vs* Fe_2O_3. (B) LOI *vs* MnO. (C) Al_2O_3 *vs* K_2O. (D) Al_2O_3 *vs* TiO_2.

MnO and Fe_2O_3 are closely related with carbonate phases, with a stronger carbonate control on MnO than Fe_2O_3, and that the alkali earth elements are associated with both carbonate and silicate minerals.

The studied, c. 40 m thick interval of the Ntombe Formation (Fig. 2) is characterized by fine to very fine grained, dark to light grey and green sandstone (from several cm to 1 m thick) interbedded with dark to light grey and green shale and siltstone (from several cm to 6 m thick) (Figs. 2 and 3; samples 92.8, 66.1 and 65.5). Sandstone shows planar bedding, current ripple lamination, normal graded bedding, load casts and mud drapes that are locally reworked and form intraclasts (e.g. sample 92.8 in Fig. 3). Shale and siltstone layers show planar and current ripple lamination, lenticular and wavy bedding, load casts, desiccation cracks, and carbonate concretions (e.g. Fig. 3E, samples 66.1, 65.5, 72.75 in Fig. 3). This suggests deposition of the studied part of the Ntombe Formation in a tidally influenced, shallow subtidal environment with episodic exposure. Intraclasts of Mn rich mud drapes are abundant in the lower part of the Ntombe Formation, representing a 6 m thick interval situated between 90.5 and 96.5 m (Fig. 2). The association of these Mn rich intraclasts with a tidally influenced marine environment illustrates Mn precipitation in shallow marine waters. Moreover, laminae of host shale are draped around Mn rich carbonate concretions (e.g. Fig. 3E, sample 65.5 in Fig. 3), illus

Table 2
Chemical composition (major elements) of different type of facies in the Ntombe Formation.

Sample N°	66.1	66.67	66.97	67.17	71.38	71.92	72.75	81.75	89.44	90.08	92.5	92.6	92.8	93.1-1	93.1–2	97.29
Host rock	1NA	1A	1A	1NA	1NA	1NA	1NA	1NA	4NA	4A	1NA	1A	4A	1A	4A	4NA
SiO_2	56.11	32.26	31.88	58.64	40.01	33.72	39.52	51.89	53.81	51.01	51.48	50.00	59.80	51.39	47.05	74.12
Al_2O_3	7.28	7.86	7.54	13.48	10.57	8.40	9.05	14.92	11.59	5.83	11.47	15.82	1.95	11.30	6.35	8.62
Fe_2O_3	19.84	24.49	30.31	11.45	23.74	29.34	23.74	14.53	12.51	19.74	16.16	14.60	14.18	15.23	18.93	5.60
MnO	4.56	14.57	8.35	1.71	5.71	6.75	6.39	2.88	5.07	7.90	5.66	4.33	13.34	8.38	15.16	0.14
MgO	0.32	1.91	2.94	2.07	3.38	3.70	2.98	3.05	2.39	4.02	0.38	4.01	4.01	4.55	1.09	2.65
CaO	2.34	0.93	1.75	0.52	0.39	0.44	0.57	0.27	0.64	0.89	4.08	0.20	0.75	0.37	3.12	4.51
Na_2O	0.33	0.07	<dl	0.05	0.12	0.08	0.27	<dl	<dl	<dl	0.02	<dl	<dl	<dl	<dl	1.20
K_2O	0.49	2.57	0.65	3.85	1.69	0.63	1.57	3.53	3.34	1.06	3.23	4.20	0.34	3.08	1.64	1.11
TiO_2	0.2	0.23	0.28	0.52	0.42	0.32	0.38	0.70	0.52	0.22	0.35	0.70	0.12	0.60	0.36	0.60
Cr_2O_3	<dl	<dl	<dl	<dl	<dl	<dl	<dl	0.06	<dl	<dl	<dl	0.06	<dl	0.05	<dl	<dl
P_2O_5	0.08	<dl	<dl	0.06	<dl	<dl	<dl	<dl	<dl	<dl	0.05	0.06	<dl	0.06	<dl	0.09
LOI*	8.39	13.4	14.2	6.3	13.1	15.8	14.5	7.3	8.7	8.1	6.94	5.0	4.2	3.9	5.40	0.8
Total	99.96	98.29	97.90	98.65	99.13	99.18	98.97	99.13	98.57	98.77	99.85	98.98	98.69	98.91	99.16	99.44
$MnO/(MnO + Fe_2O_3)$	0.19	0.37	0.22	0.13	0.19	0.19	0.21	0.17	0.29	0.29	0.26	0.23	0.48	0.35	0.44	0.02

Major element concentrations obtained by XRF in wt.%. 1NA = unaltered carbonate-rich shale; 1A = altered carbonate-rich; 4NA = unaltered argillaceous sandstone/siltstone; 4A = altered argillaceous sandstone/siltstone. * = LOI (lost on ignition) after 30 min at 930 °C in air; <dl = concentration below the detection limit of 0.05 wt.%.

trating a pre compactional formation of the concretions. In view of this, the concretions formed from precipitation and lithification process during early diagenesis.

Shales of the Sinqeni and Ntombe formations show a foliation at an angle to bedding, which is developed on a regional scale in the White Umfolozi Inlier, possibly associated with folding of the Pongola Supergroup along a NE trending axis (Figs. 1, 3F). The timing of this folding is unclear, but it may have formed during the regional event of deformation metamorphism that took place in the late Archaean (Elworthy et al., 2000) or, alternatively, during deformation related to the c. 1.0 Ga Namaqua Natal orogeny (Eglington, 2006) that affected the southern Kaapvaal Craton margin situated

c. 60 km to the south of the White Umfolozi Inlier (Fig. 1).

Both sandstone and shale show some evidence of alteration near fracture networks showing two main geometries (Fig. 3F), (1) sub vertical and perpendicular to the foliation, and (2) subhorizontal and parallel to the foliation. Aureoles of alteration are sometimes developed on both sides of the fractures illustrated by a change of host rock's color. Similar to the Vlakhoek Member, we differentiate unaltered and altered intervals, the latter showing fracture networks with or without alteration haloes. The average of MnO content across the studied c. 40 m thick interval of the Ntombe Formation (Fig. 2) is 6.93 wt.%. In samples from unaltered domains, MnO is up to 6.7 wt.%, whereas concentrations up to 15.2 wt.% may be reached in altered samples (Table 2). These values are much higher than the average value of the Mozaan Group shale at 0.16 wt.% (Wronkiewicz and Condie, 1989). In samples from both Sinqeni and Ntombe formations, the highest concentrations of MnO associated with unaltered rocks have been recorded in carbonate rich layers and early diagenetic concretions. Except for a few samples, MnO/Fe_2O_3 ratios range from 0.1 to 0.5 with an average of 0.4 (Table 2). This ratio is much higher than that of Archean Fe rich mudrocks at 0.025 and the crustal average at 0.022 (Lepp, 2008). Co variations exist in the concentration of some major elements. Fe_2O_3 shows a strong positive co variation (R^2 = 0.89) with LOI, suggesting that Fe_2O_3 content could be mainly associated with carbonate phases. In contrast, MnO shows a very weak positive co variation (R^2 = 0.19) with LOI, whereas samples with the highest MnO contents illustrate a weak relationship between LOI and MnO (Fig. 4). SiO_2 and Al_2O_3 contents vary between 32 and 60 wt.% and 5 and 16 wt.%, respectively (Table 2), with the higher concentrations being close to average Mozaan Group shale at 60.9 wt.% and 17.5 wt.% respectively (Wronkiewicz and Condie, 1989). SiO_2/Al_2O_3 ratios are mostly between 3 and 9, except for sample 92.8 with a value of about 30 (Table 2). Lower ratios suggest a predominance of clay minerals, whereas a dominance of quartz sand is indicated for sample 92.8. The strong co variation (R^2 = 0.86) observed between Al_2O_3 and K_2O (Fig. 4) suggests a possible increase of aluminous phases (phyllosilicates) together with K. According to Veizer and Garrett (1978), these Al rich phases plot between the illite muscovite sericite and montmorillonite fields, although much closer to the illite trend (Fig. 4). The positive correlation between Al_2O_3 and TiO_2 (Fig. 4) illustrate an enrichment of Ti together with Al rich phases, suggesting that these Al rich phases may be clay minerals rather than muscovite, orthoclase or microcline (Veizer, 1978). P_2O_5 values are below 0.09 wt.% (Table 2), indicating the subordinate presence of phosphate phases.

4.2. Petrography and mineral chemistry

4.2.1. Unaltered rocks of the Sinqeni Formation

BIF is characterized by carbonate rich layers interbedded with silica and iron oxide rich layers (Fig. 5A C). Carbonate rich layers and concretions contain between about 60 and 70 vol.% car bonate (Fig. 5C). The carbonate phases that represent the main Mn host minerals are essentially siderite and kutnohorite with more than 8 and 17 wt.% of MnO, respectively (Table S2). The latter mineral assemblage is observed together with magnetite, quartz, as well as some ankerite and calcite (Fig. 5C, Table S2). Considering that Mn rich siderite, kutnohorite and ankerite are associated with carbonate concretions, they appear to have formed prior to compaction, probably during early diagenesis. According to these observations, the manganese content in unaltered Sinqeni rocks (including BIFs and green shale), reaching 8.5 wt.% MnO, reflects syn sedimentary to early diagenetic processes of enrichment. Beside the carbonates, chlorite is observed associated with the metamorphic fabric (foliation, Fig. 5D) in BIF.

4.2.2. Altered rocks of the Sinqeni Formation

Samples are dominated by products of alteration processes driven by fluid circulations (Fig. 5E H). Mineral phases formed during these processes involve Mn siderite, rhodochrosite, Fe Mn chlorite, ankerite, hematite, quartz and pyrite (Fig. 5E H, Table S2). The Mn sid phase shows MnO contents above 18 wt.%, and much higher than the average of 8.7 wt.% recorded in the unal tered rocks, illustrating Mn enrichment during alteration (Table S2). Mn siderite/ankerite/quartz veins are observed in asso ciation with a fracture network cross cutting another fracture net work filled by pyrite (Fig. 5E and F). The presence of hematite also associated with fractures suggests a possible late circulation of more oxidized fluids (Fig. 5G). In these samples, MnO content

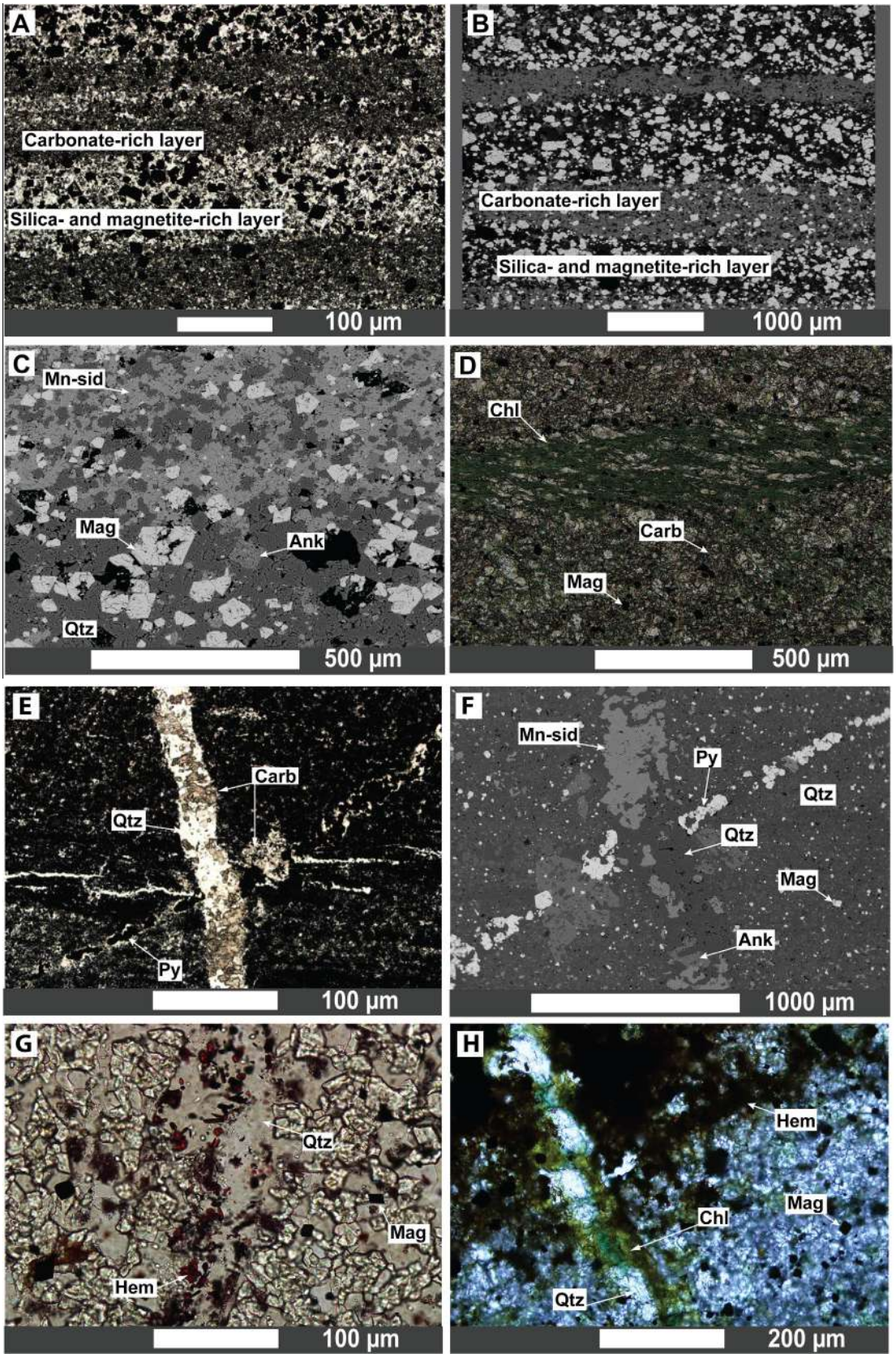

Fig. 5. Characterization and relationship between mineral phases in the Sinqeni Formation. (A and B) Photomicrograph and backscattered electron image of carbonate-rich lamina interlayered with silica- and iron oxide-rich lamina. (C) Backscattered electron image of carbonate- and silica-rich lamina showing manganoan siderite, ankerite, quartz and magnetite; carbonate abundance may reach about 60–70%. (D) Photomicrograph showing foliation domain of chlorite in a carbonate- and magnetite-rich sample. (E and F) Photomicrograph and backscattered electron image showing fractures filled with carbonate (manganoan siderite and ankerite), quartz and pyrite. (G and H) Photomicrograph showing fracture filled by quartz and chlorite controlling the transformation of magnetite to hematite. (Mn-sid: manganoan siderite; Mag: magnetite; Ank: ankerite; Qtz: quartz; Chl: chlorite; Carb: carbonate; Py: pyrite; Hem: hematite).

may be as high as 11.3 wt.% (Table 1), suggesting slight Mn enrich ment during alteration.

4.2.3. Unaltered rocks of the Ntombe Formation

The Fe Mn rich mineral phases are dominated by carbonates associated with chlorite and scattered euhedral pyrite (Fig. 6A and B). Most carbonate phases are Mn rich, including manganoan siderite (Mn sd, Fig. 6; Table 3), which is associated with ferroan rhodochrosite (Fe rds, Fig. 6E, S3; Table 3), and a Ca rich carbonate with a Mn/Fe ratio greater than 1, the composition of which is close to kutnohorite (Fig. 6C and D; Table 3). The Ferds phase is characterized by a Mn/Fe ratio greater than 1 (Table 3). It occurs as remnants in the center of euhedral crystals marginally replaced by anhedral to subhedral Mn sd, suggestive of a later diagenetic or metamorphic replacement (Fig. 6E and F). Mn sd has a Mn/Fe ratio smaller than 1 (Table 3). As shown with unaltered rocks of the Sinqeni Formation, it appears that carbonate phases are the main Mn hosting minerals. However, their relationship with intraclasts of mud drapes, carbonate concretions and carbon ate layers suggest a syn sedimentary and/or early diagenetic origin of Mn rich mineral precursors of Mn rich carbonate phases. This suggests that the MnO content, as high as 6.7 wt.% (Table 2), recorded in the unaltered rocks is also probably a primary (i.e. sedimentary or early diagenetic) constituent of the Ntombe Forma tion. Moreover, the presence of chlorite forming the metamorphic fabric together with Mn sd (Fig. 6A and B) probably supports metamorphic overprinting of an earlier Fe rds phase. This metamorphic chlorite is a Fe rich phase with Mn content lower than 1 wt.% (Table 3).

4.2.4. Altered rocks of the Ntombe Formation

The altered rocks were affected by late fluid circulation, as veins filled with Mn Fe rich mineral phases are usually cross cutting the metamorphic fabric or earlier formed mineral occurrences (Fig. 7A and B). Alternatively, some deformed veins cross cutting the metamorphic fabric may also suggest that they formed during the deformation that gave rise to the observed metamorphic fabric (Fig. 7A). Two different mineral associations can be recognized (Figs. 7 9): (1) carbonate silicate phyllosilicate, and (2) carbon ate oxide phyllosilicate associations.

4.2.4.1. Carbonate silicate phyllosilicate association. In the meta morphic fabric, Fe tephroite is associated with cronstedtite, Fe Mn chlorite, rhodochrosite and pyrophanite (Fig. 7A C, S4; Tables 4, S1). Early metamorphic Fe chlorite and phlogopite seem to be partially replaced by Fe Mn chlorite, Fe tephroite and cronstedtite in the metamorphic fabric (Fig. 7B and C). In the altered intraclasts of reworked mud drapes, the mineral assemblage is characterized by Fe tephroite, rhodochrosite, Fe Mn chlorite and Mn phlogopite (Fig. 7D F, S4; Tables 4, S1) and rarely illite (Fig. 7D F). As fracture fillings, Ca rhodochrosite is associated with Fe tephroite, cronst edtite, quartz, Fe Mn chlorite and Mn phlogopite (Figs. 7A, 8, S4; Tables 4, S1).

Rhodochrosite associated with the metamorphic fabric is compositionally close to the rhodochrosite end member (e.g. 1A, Table 4), whereas in the altered mud intraclasts and in the fracture fillings it is Ca rich (e.g. 2A, Table 4). Both types have FeO contents between 1 and 3 wt.%. MnO and FeO contents of Fe tephroite associated with the metamorphic fabric are as high as 30 and 15 wt.%, respectively (e.g. 1A, Table 4), while those from intraclasts and fracture fillings are as high as 34 and 27 wt.%, respectively (e.g. 2A, Table 4). Cronstedtite, both in the metamorphic fabric and fracture fillings has FeO content up to 82 wt.% and MnO reaching 6 wt.% (Table 4). Three types of chlorite have been observed: (1) chlorite type 1, which is the earliest Fe chlorite characterizing the metamorphic fabric with MnO content lower than 1 wt.% (Fig. 7B and C, Table 4), (2) chlorite type 2, represented by Fe Mn chlorite with MnO contents between 1 and 3 wt.% and partially replacing chlorite type 1, (e.g. 1A and 2A matrix in Table 4; Fig. 7B and C), and (3) chlorite type 3 with MnO contents as high as 7 wt.% and associated with mud intraclasts and fracture fillings (e.g. samples 1A and 2A frct in Table 4; Figs. 7D F, 8D). Chemical variations are also observed in the phlogopite phase. Phlogopite from metamorphic fabric domains has an FeO content reaching 4 wt.% and MnO content lower than 1 wt.% (e.g. 1A, Table 4). Phlogopite associated with fracture fillings and intraclasts is unusually Fe and Mn rich (Mn phlogopite) (e.g. 2A, Table 4, and as shown by Raman spectroscopy analyses in Text SI, Fig. S3 and Table S1). Following these observations, a mineral diversification is observed from unaltered to altered rocks. This mineral diversification, controlled by fluid circulation, is accompanied by local Mn remobilization and enrichment, where the MnO content may reach up to 15.2 wt.% in altered rocks (Table 2).

4.2.4.2. Carbonate oxide phyllosilicate association. Mn Fe bearing oxide mineral phases are dominated by pyrochroite (Fig. 9A and B, S3; Table S1), rarely associated with a Fe Mn rich oxide phase showing a Mn/Fe ratio lower than 1 similar to jacob site (Fig. 9C and D; Table 4). Both pyrochroite and jacobsite seem to replace previous carbonate phases characterized by Fe rds, Mn sd and kutnohorite as shown in Fig. 9D. This alteration is found along fractures to form an alteration halo. Pyrochroite has a MnO content as high as 77 wt.% and a FeO content lower than 1 wt.%, whereas jacobsite is characterized by a FeO content of up to 64 wt.% and MnO reaching 14 wt.% (Table 4). Pyrophanite occurs both in the metamorphic fabric and mud intraclasts (Figs. 7B, 9E and F). It replaces rutile crystals as indicated by frequent marginal replacement (Fig. 9E and F). Its MnO and FeO contents may be as high as 11 wt.% and 33 wt.%, respectively (Table 4). Fe Mn carbon ates are by far the dominant phase within the studied samples and include Mn sd, Fe rds and kutnohorite. Pyrochroite, jacobsite and pyrophanite were the identified oxide phases. Observed alteration processes controlled by fluid circulation show mineral diversification and Mn enrichment from unaltered to altered rocks where MnO may reach 14.6 wt.% (Table 2).

4.3. Thermodynamic modeling on chlorite and thermal conditions

The three types of chlorite described in this study are associated with Mn Fe rich mineral phases that formed during metamorphism and fluid circulation. Therefore, to constrain under which thermal conditions these mineral phases formed, thermodynamic modeling has been carried out based on the chemical composition of chlorite phases. Calculations were done on the basis of 14 oxy gens and plotted in the vector representation diagram of Wiewiora and Weiss (1990) that usually characterize crystallo chemical properties of chlorites. The studied chlorites are triocta hedral with a number of silicon atoms below 3.25 (with a majority below 3) per formula unit and an octahedral charge ranging between 5.5 and 6 (Fig. 10A). Additionally, according to the trian gular plot of Velde (1985), these chlorites are Fe rich, situated in the theoretical field of metamorphic to hydrothermal chlorites (Fig. 10B). Several thermodynamic models based on chemical com position of chlorite have been published (e.g. Walshe, 1986; Vidal et al., 2005, 2006; Inoue et al., 2009). However, the redox state of Fe from Fe rich chlorite is likely to influence the distribution of other elements in the crystalline structure of chlorite as well as its formation temperature. Indeed, the temperature estimate of Fe rich chlorite derived by thermodynamic modeling could be wrong if the Fe^{3+} content is not considered. Most of these pub lished models do not consider Fe^{3+} contents. The model of Vidal et al. (2005, 2006), based on multiple equilibria, can be used for

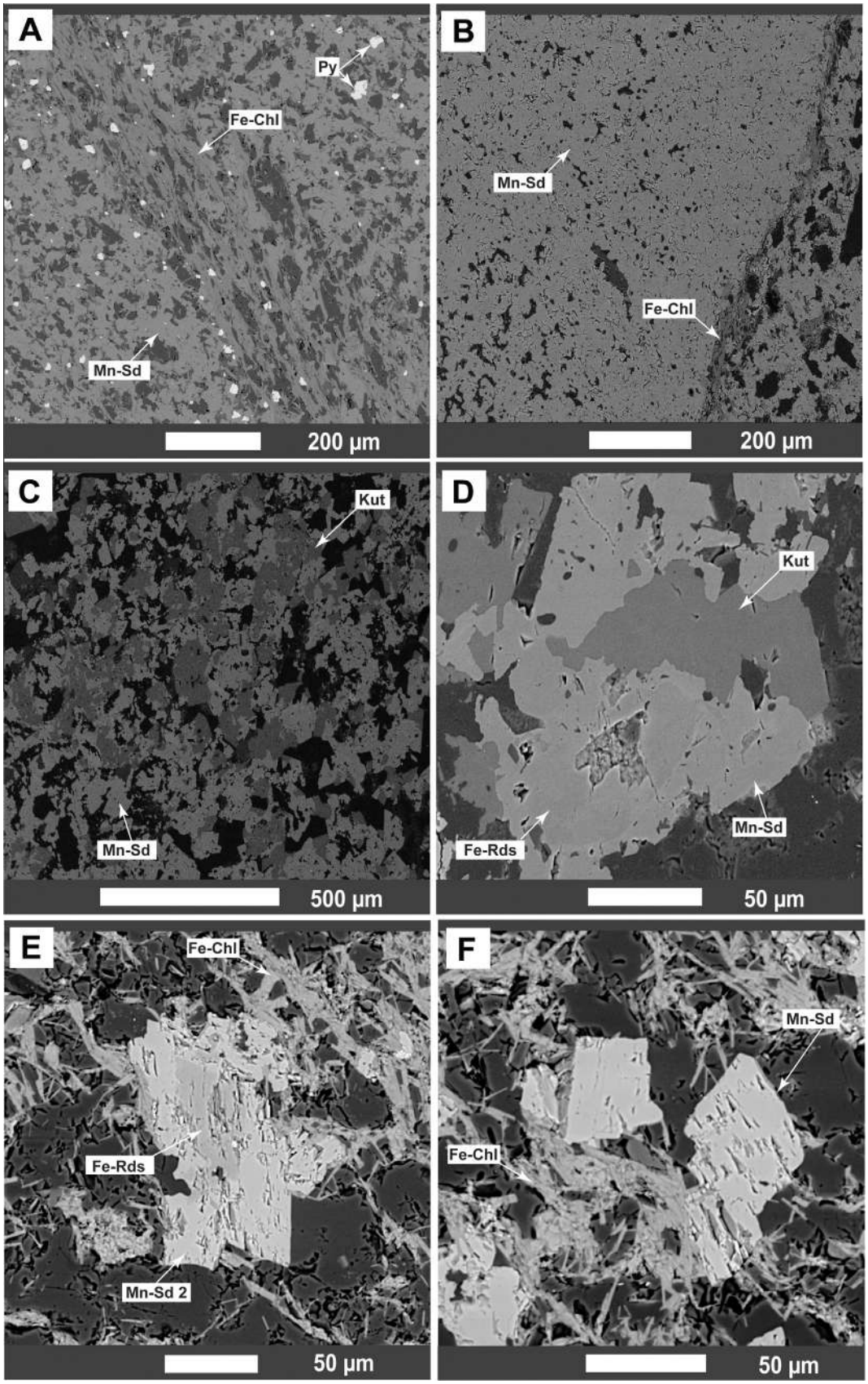

Fig. 6. Characterization and relationship between mineral phases within unaltered rock of the Ntombe Formation. (A and B) Backscattered electron images of carbonate-rich shale bed characterized by manganoan siderite (Mn-sd) and Fe-rich chlorite (Fe-Chl) in foliation domains. Note disseminated euhedral pyrite in A. (C) Backscattered electron image showing carbonate-rich bed characterized by manganoan siderite (Mn-sd) associated with kutnohorite (Kut). (D and E) Backscattered electron images of euhedral ferroan rhodochrosite (Fe-rds) marginally replaced by coarse anhedral to subhedral manganoan siderite (Mn-sd) 2). (F) Backscattered electron image of an anhedral to euhedral Mn-sd.

Table 3
Chemical composition of Mn–Fe-rich mineral phases in unaltered rock of Ntombe Formation.

Mineral	Chlorite		Fe-rhodochrosite	Mn-siderite		Kutnohorite
Theoretical formulae	$(Mg,Fe)_3(Si,Al)_4O_{10}$		$FeMnCO_3$	$MnFeCO_3$		$CaMn^{2+}(CO_3)_2$
Average of N	29	45	26	26	17	12
Host rock	1NA	4NA	1NA	1NA	4NA	1NA
SiO_2	27.77	26.05	0.10	0.09	0.18	0.08
Al_2O_3	24.53	23.29	0.02	0.01	0.09	0.01
FeO	39.00	44.08	21.71	36.55	38.57	11.43
MnO	0.84	0.34	30.33	17.54	16.78	13.71
MgO	7.00	5.80	6.33	4.53	0.89	5.47
CaO	0.05	0.07	1.03	1.02	4.10	26.09
Na_2O	0.04	0.07	nd	nd	nd	nd
K_2O	0.03	0.06	nd	nd	nd	nd
TiO_2	0.65	0.12	nd	nd	nd	nd
Cr_2O_3	0.06	0.11	nd	nd	nd	nd
CO_2	nd	nd	40.40	40.18	39.32	42.95
Total	99.99	100	99.92	99.92	99.92	99.74
MnO/FeO	nd	nd	1.40	0.48	0.44	1.20

Major element concentrations obtained by EPMA in wt.%. 1NA = unaltered carbonate-rich shale facies; 4NA = unaltered argillaceous sandstone/siltstone facies. N = number of analyses; nd = not determined.

metamorphic and/or hydrothermal chlorites which have a number of silica (Si) atoms less than 3 per formula unit, calculated on the basis of 14 oxygens. This model offers an adjustment of crystalliza tion temperature by varying Fe^{3+} contents of chlorites (Vidal et al., 2005, 2006) and appears best suited for this study. By applying this model, the calculated equilibrium temperatures range between 450 and 265 °C (average of 310 ± 54 °C) for chlorite type 1, 320 and 180 ° C (average of 264 ± 34 °C) for chlorite type 2, and 290 and 150 °C (average of 244 ± 41 °C) for chlorite type 3 (Fig. 10C). Note that the average of estimated temperatures of the different chlorite types decrease firstly from early metamorphic to late metamorphic chlorite, and secondly from the latter to chlorite phases related to late fluid circulations.

4.4. $^{40}Ar/^{39}Ar$ dating K rich clay fraction

Results of $^{40}Ar/^{39}Ar$ dating performed on K rich phyllosilicate phases from samples 93.1, 162.4 and FR7 are shown in Fig. 11 and listed in Table S3. Considering that grain sizes of the clay fraction might not be more than an order of magnitude greater than the length of recoil path of ^{39}Ar nuclei produced in irradiation

~80 nm, Villa, 1997), the use of $^{40}Ar/^{39}Ar$ dating on K rich clay minerals may be viewed with skepticism. Indeed ^{39}Ar might be partially lost during irradiation resulting in an apparent age that can be too high.

However, reimplantation of the recoiled nuclei into adjacent grains occurs in a dense aggregate and under vacuum (Huneke and Smith, 1976). In the case of monomineralic aggregates, realistic plateau ages can result (Dong et al., 1995, 1997). Further, ^{39}Ar loss by recoil in a fine grained aggregate tends to present as a "hump" in the age spectrum, with low temperature steps particu larly showing high ages, and a lower age plateau being approached at higher temperature releases (McDougall and Harrison, 1999). Such patterns are not observed in the present study, and therefore there is no positive indication of recoil loss. Instead, the dating experiments yield age spectra with step ages increasing with step temperature (staircase patterns). In one case (sample 93.1, Fig. 11), the higher temperature steps produce a near plateau with an integrated age of 1433 ± 8 Ma (an integrated age results from virtually remixing the argon released in the included steps and calculating an age from the aggregate). The other two samples yield more irregular high temperature age patterns over smaller fractions of cumulative ^{39}Ar. These three results do not constitute an age deter mination in the strict sense. However, their broad consistency in the range 980 1490 Ma, half the age of the Mozaan Group, indi

cates that the thermal event controlling mineral transformation and diversification associated with Mn remobilization and enrich ment was a late, separate event not related to diagenesis and probably also not to the burial phase.

5. Discussion

5.1. Nature and origin of Mn in the Mozaan Group

The Fe Mn rich mineral phases from BIFs and shales of the Sinqeni and Ntombe formations are represented by carbonates, orthosilicates, oxides, phyllosilicates and pyrite (Fig. 12). Similar mineral assemblages are common within iron manganese ore fields (e.g. Bajoumy et al., 2012; Gutzmer and Beukes, 1995; Lucchetti, 1991; Mossman and Pawson, 1976; Öztürk, 1997; Zaitsev, 1996). The thermal evolution experienced by unaltered rocks seems to have been controlled by both burial diagenesis and metamorphism. The MnO content of BIFs and shales is up to 8.5 and 6.7 wt.%, respectively (Tables 1 and 2). In the unaltered rocks, Mn sd, Fe rds and kutnohorite appear as the main Mn host minerals, and their abundance may be as high as 90 vol.% in thin carbonate rich layers and early diagenetic carbonate concre tions. Petrographic investigation (e.g. Fig. 6) shows the Fe rds as the earliest mineral phase subsequently replaced by Mn sd later during diagenesis and/or metamorphism. Additionally, a common occurrence of these two mineral phases associated with intraclasts of reworked mud drapes, early lithified carbonate concretions and thin carbonate rich beds (see in Fig. 3) supports a syn sedimentary and/or early diagenetic origin of Mn rich mineral precursors of Fe rds and Mn sd. Therefore, Mn phases precipitated in shallow mar ine and early diagenetic environments. In view of this, Mn can be regarded as a primary constituent related to the sedimentation of the Mozaan Group.

In marine environments, Mn and Fe are mainly supplied by hydrothermal processes and continental runoff (Roy, 2006). Although marine hydrothermal systems are thought to have been the main sources of Mn and Fe during the Archean Eon (Holland, 2002; Roy, 2000, 2006), a contribution from continent derived solutes cannot be discounted for sediments that formed in an intracontinental setting such as the Pongola basin. Indeed, rare earth element (REE) patterns and Nd isotope ratios of the Sinqeni IF suggested that continental derivation of Nd (so potentially Nd Fe coupling) to seawater was significant (Alexander et al., 2008). On the basis of REE systematics, Delvigne et al. (2012)

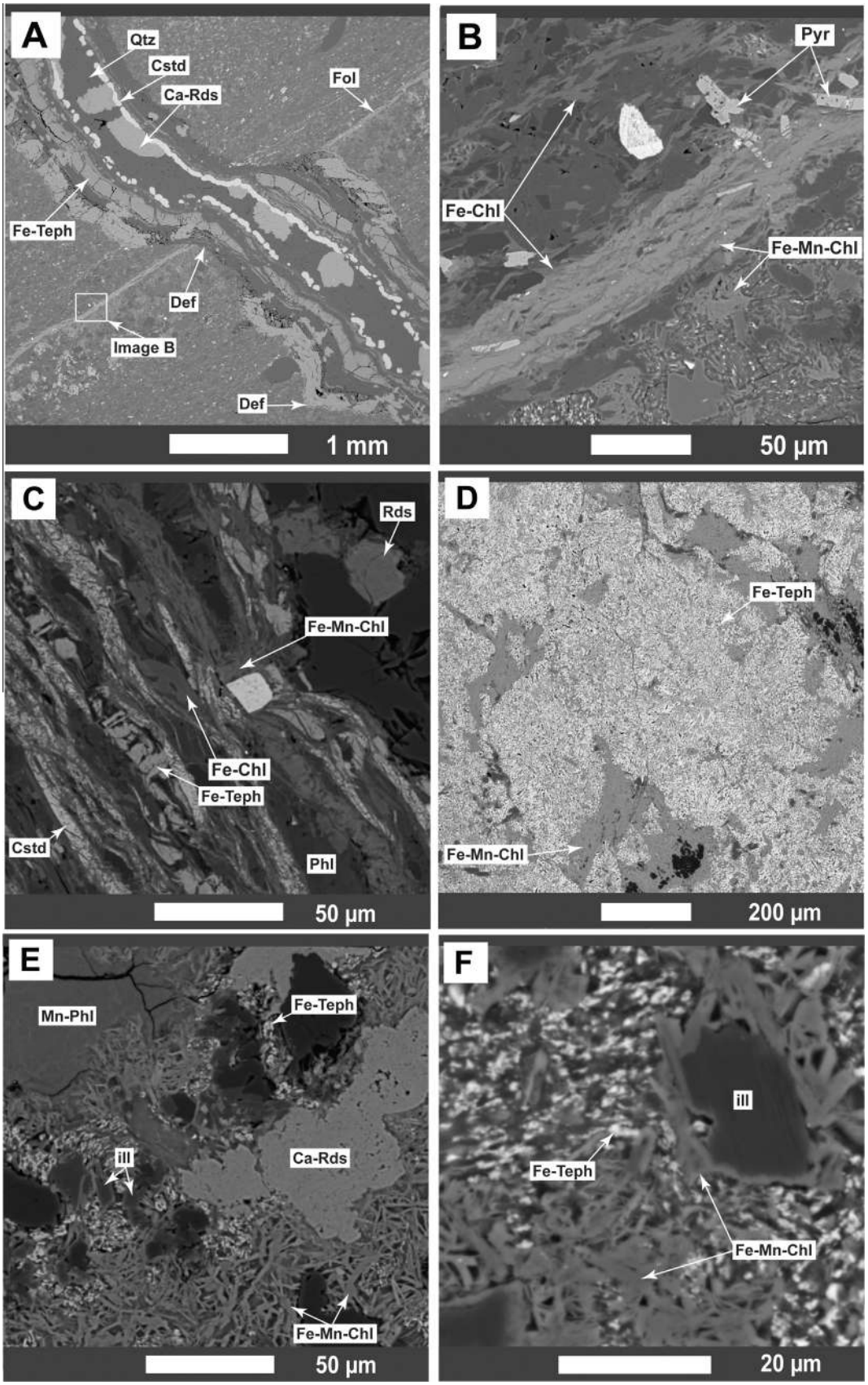

Fig. 7. Carbonate–silicate–phyllosilicate mineral association in altered rock related to fracture network. (A) Backscattered electron image of deformed vein filled by Mn–Fe-rich minerals and quartz. (B and C) Backscattered electron images of late metamorphic phases, including Fe–Mn-chlorite (Fe–Mn-Chl or chlorite type 2), pyrophanite (Pyr), cronstedtite (Cstd) and rhodochrosite (Rds) partially replacing early metamorphic phases that include Fe-chlorite (Fe-Chl or chlorite type 1) and phlogopite (Phl) defining the metamorphic fabric; location of B shown in Fig. 7A. (D–F) Backscattered electron images showing early metamorphic phases (e.g. illite) partially to totally replaced by ferroan tephroite (Fe-teph), Fe–Mn-chlorite (Fe–Mn-Chl or chlorite type 3), rhodochrosite (Rds) and manganoan phlogopite (Mn-Phl). (Ca-Rds: calcian rhodochrosite; ill: illite).

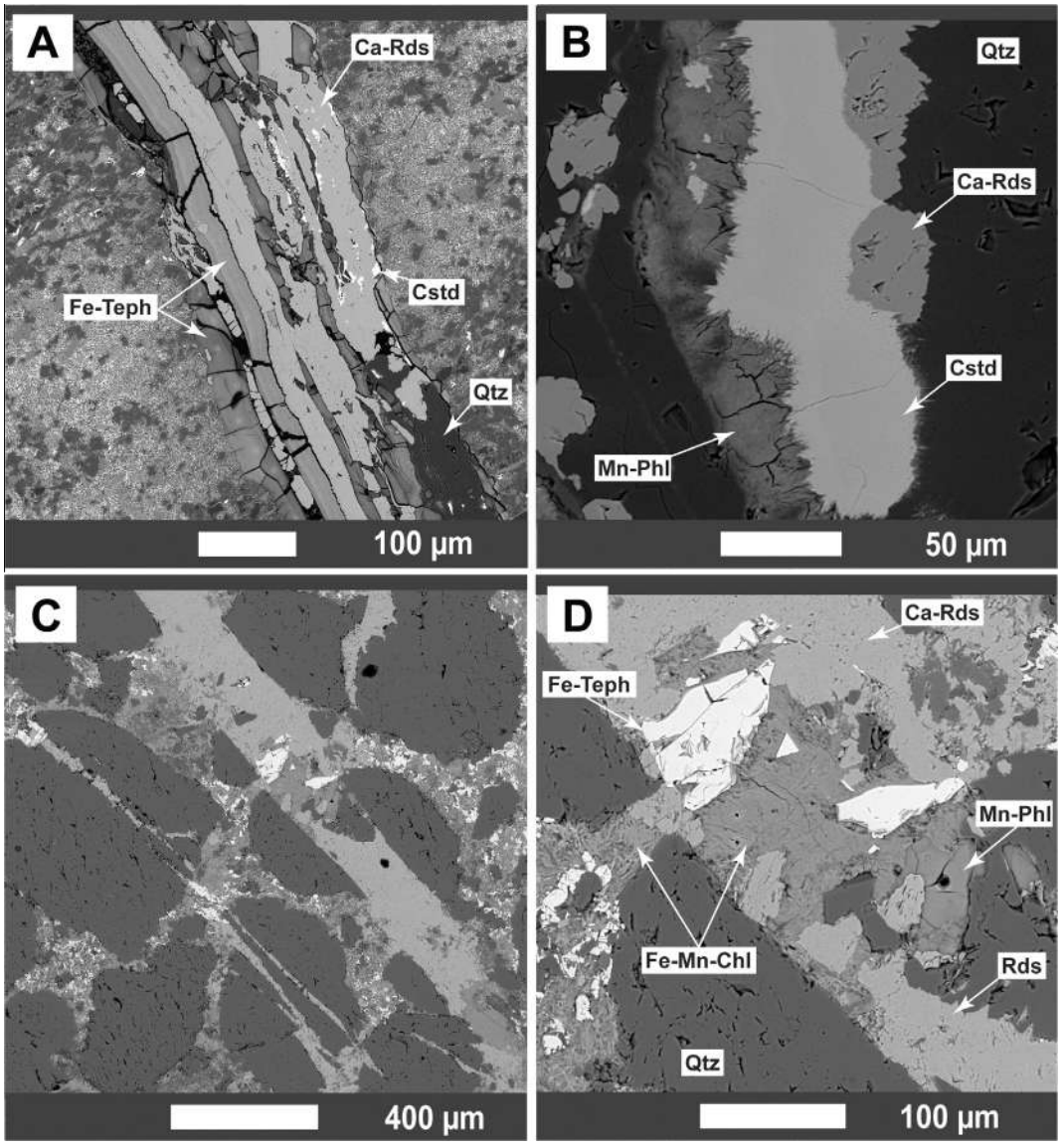

Fig. 8. Carbonate–silicate–phyllosilicate mineral assemblage associated with fracture infills of altered rocks. (A and B) Backscattered electron images of fracture fillings characterized by ferroan tephroite (Fe-Teph); rhodochrosite (Rds); cronstedtite (Cstd); manganoan phlogopite (Mn-Phl) and quartz (Qtz). (C and D) Backscattered electron images showing Rds associated with Fe-Teph, Fe–Mn-chlorite (Fe–Mn-Chl or chlorite type 3) and Mn-Phl as fracture fillings.

argued for the presence of a minor (ca. 10%) freshwater component in the depositional basin of the Sinqeni BIF.

Elevated Mn and Fe contents of unaltered rocks of the Mozaan Group are mainly associated with carbonate phases. It is thought that the precipitation of Archean BIFs was a result of either Fe^{2+} oxidation due to free oxygen derived from photosynthetic activity, or anaerobic Fe^{2+} oxidation by photo autotrophs (Holland, 2005; Konhauser et al., 2002). However, two hypotheses may be considered in the case of Mn precipitation in the Archean. The first hypothesis was proposed by Johnson et al. (2013) and is similar to the photo ferrotrophy model of Konhauser et al. (2002). It argues that the water oxidizing complex of photosystem II evolved from a former transitional photosystem, where anoxygenic photo biology used Mn as an electron donor (photo oxidation of Mn^{2+}). In the second hypothesis, the precipitation of Mn by oxidation of aqueous Mn(II) to Mn(III/IV) was driven by free O_2 present in "oxy gen oases" supplied from localized photosynthetic activity in basin margin photic zones (Kasting, 1993). Because the photo chemical oxidation of Mn^{2+} would be inhibited in the presence of Fe^{2+} (Anbar and Holland, 1992), it appears that oxygenic photosyn thesis would be regarded as the main control of Mn precipitation in seawater during the deposition of the Mn Fe rich rocks of the Mozaan Group. This may be supported by the presence of stromatolitic carbonates in the Nsuze Group of the White Umfolozi Inlier, regarded to have been formed by photosynthetic organisms (Beukes and Lowe, 1989; Siahi et al., 2016), as well as filamentous microstructures resembling fossilized cyanobacteria observed in the Ntombe Formation (Noffke et al., 2003). Examining a paleosol developed below the Mozaan basal unconformity and Vlakhoek Member BIFfrom the White Umfolozi Inlier, Crowe et al. (2013) reported mobilization of redox sensitive elements (Cr, U) and fractionation of Cr isotopes interpreted to reflect oxidative weathering. Crowe et al. (2013) thus argued for the presence of appreciable amounts of free O_2 in the atmosphere (3×10^{-4} times present day levels) 3 billion years ago. Furthermore, BIF and shale samples of the Sinqeni Formation, including some of the present study, show a positive correlation between Fe/Mn ratios and Mo isotope values (Planavsky et al., 2014). Large fractionations of Mo isotopes

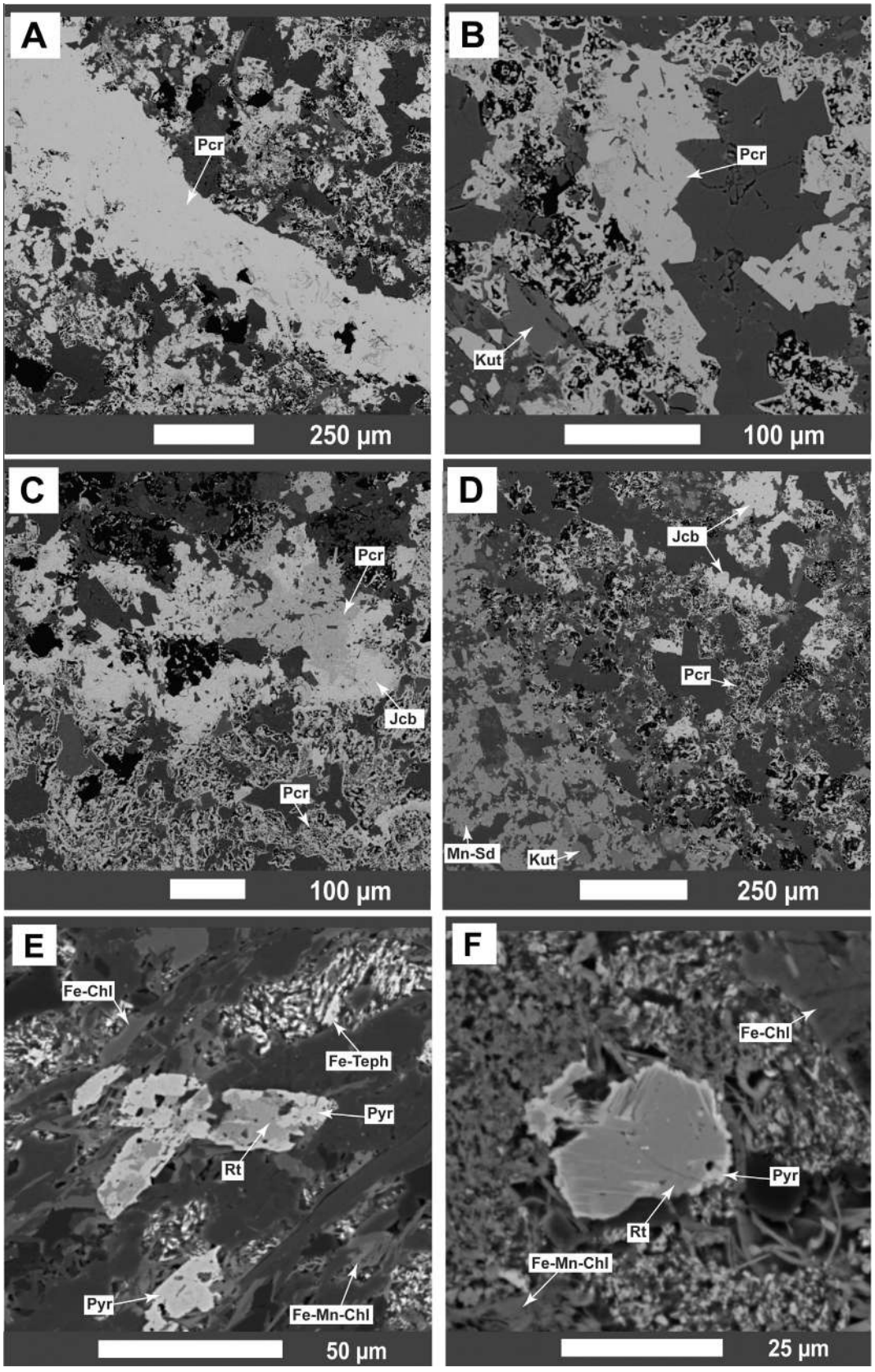

Fig. 9. Carbonate–oxide–phyllosilicate mineral assemblage associated with fracture infills of altered rocks. (A-D) Backscattered electron images showing early carbonate phases, Mn-Sd 2 and kutnohorite (Kut), partially or totally replaced by late pyrochroite (Pcr) and jacobsite (Jcb). (E-F) Backscattered electron images of rutile (Rt) showing pyrophanite (Pyr) overgrowths. (Fe-Chl: ferroan chlorite; Fe-Teph: ferroan tephroite; Fe–Mn-Chl: manganoan Fe-rich chlorite).

Table 4
Chemical composition of Mn–Fe-rich mineral phases in altered rock of Ntombe Formation.

Mineral	Fe-tephroite	Cronstedtite*	Rhodochrosite	Pyrophanite		Chlorite				Phlogopite			Pyrochroite	Jacobsite
Theoretical formulae	$(Fe,Mn)_2SiO_4$	$Fe^{2+}_2Fe^{3+}$ $(Si,Fe^{3+}O_5)(OH)_4$	$MnCO_3$	$MnTiO_3$		$(Mg,Fe)_3(Si,Al)_4O_{10}$				$KMg_3AlSi_3O_{10}(F,OH)_2$			$Mn(OH)_2$	$MnFe_2O_4$
Average of N	18	21	12	19		35	19	16	12	14	15	8		7
Host rock	1A	4A	1A	4A	1A	4A	1A (mtx)	1A (frct)	4A (mtx)	4A (frct)	1A	4A	1A		1A
SiO_2	48.49	32.12	9.80	0.10	1.47	1.17	1.53	29.70	32.46	30.11	32.67	50.61	52.87	0.27	2.76
Al_2O_3	0.78	0.06	0.03	0.00	0.18	0.13	0.00	23.65	19.77	22.65	18.65	31.55	22.92	0.14	0.15
FeO	14.70	26.61	82.17	1.10	2.49	11.10	4.10	30.68	30.25	29.38	28.92	3.79	7.22	0.08	64.32
MnO	30.23	33.93	6.39	50.58	47.65	33.30	22.33	1.77	5.72	2.12	6.88	0.70	4.89	77.30	13.54
MgO	4.36	6.72	1.38	0.24	0.52	0.14	0.22	13.85	10.86	15.20	11.83	1.82	2.56	0.03	0.12
CaO	1.37	0.34	0.23	1.01	6.22	0.03	0.07	0.03	0.07	0.04	0.10	0.03	0.16	0.04	0.35
Na_2O	nd	nd	nd	nd	nd	nd	nd	0.00	0.00	0.00	0.00	0.00	0.05	0.01	0.01
K_2O	nd	nd	nd	nd	nd	nd	nd	0.18	0.79	0.33	0.85	10.74	7.69	0.00	0.01
TiO_2	0.01	0.03	0.01	nd	nd	53.37	71.74	0.12	0.08	0.11	0.08	0.73	0.28	nd	nd
Cr_2O_3	nd	nd	nd	nd	nd	nd	nd	0.00	0.00	0.00	0.00	0.00	0.09	nd	nd
CO_2	nd	nd	nd	46.83	41.30	nd	nd	nd	nd	nd	nd	nd	nd	nd	nd
Total	99.96	99.82	100	99.86	99.82	100	100	99.97	99.95	99.93	99.97	99.97	98.74	79.92	81.67
MnO/FeO	2.06	1.29	0.08	45.95	19.17	3.00	5.45	nd	nd	nd	nd	nd	nd	nd	0.21

Major element concentrations obtained by EPMA in wt.%. 1A = altered carbonate-rich shale facies; 4A = altered argillaceous sandstone/siltstone facies; (mtx) = clay alteration by replacement (solid state transformation) in the matrix; (frct) = clay alteration by recrystallization (dissolution-crystallization) associated with fractures. N = number of analyses; nd = not determined. Cronstedtite* = cronstedtite-like mineral phase.

was related to sorption of Mo onto Mn oxyhydroxides, the presence of which would require substantial concentrations of free oxygen in the shallow marine water and derived from oxygenic photosynthesis already established at that time (Planavsky et al., 2014). During diagenesis, Mn oxides would have then been transformed to Mn rich carbonates. Indeed, a process widely recognized for the formation of Archean and Paleoproterozoic Mn and Fe rich carbonates is the microbial induced reduction of Mn and Fe oxides (precipitated from seawater) during early diagenesis coupled to oxidation of sedimentary organic carbon, releasing Mn^{2+}, Fe^{2+} and CO_3^{2-} to form Mn and Fe rich carbonates (Johnson et al., 2013; Tsikos et al., 2003). Smith et al. (2013) inferred similar process from the depleted $\delta^{13}C_{PDB}$ values (between 17 and 9‰) of carbonate phases associated with Fe rich shale and BIFs of the stratigraphically correlative Witwatersrand Supergroup. Based on the observation that Mn precipitation in the Mozaan Group may have been related to elevated Mesoarchean O_2 levels in shallow seawater, further chemostratigraphic investigations will be necessary. Due to the presence of Neoarchaean Mn deposits in India and Brazil, it has been suggested that the introduction of photosystem II and decrease of the oxygen sinks led to a limited buildup of sur face O_2 content by the Late Archaean and initiated modest deposition of Mn in shallow basin margin oxygenated niches (Roy, 2006). Evaluating the O_2 levels of the atmosphere hydrosphere system during Meso and Neoarchaean times may thus provide new perspectives in the exploration for sediment hosted mineral deposits in the Archaean record.

5.2. Mn remobilization and enrichment processes

Assuming that Fe rds is the mineral precursor for Mn sd and kutnohorite, the difference in the Mn/Fe ratio observed between the two minerals shows that this transformation was accompanied by Mn remobilization during diagenesis and/or metamorphism (Fig. 12). Therefore, the redistribution of Mn would have probably occurred firstly between Fe rds (considered here as paragenesis (1) and early metamorphic phases (considered as paragenesis (2). The second remobilization and redistribution of Mn would have occurred during the partial or total replacement of parageneses 1 + 2 by late metamorphic mineral phases (seen as paragenesis (3). The last remobilization and redistribution of Mn is marked by intense alteration involving late fluid circulation where previ ous phases (parageneses 1 + 2 + 3) are partially or totally replaced by mineral phases related to late fluid circulation (paragenesis 4). The partial or total replacement and dissolution precipitation processes associated with variation of Mn content suggest a remobilization process of Mn within the Mozaan Group. This allows a progressive enrichment of Mn from unaltered to altered rocks during the thermal history experienced by the Mozaan Group.

Except for paragenesis 1, chlorite is observed to occur in association with all other mineral parageneses (Fig. 12). The estimated temperature of formation of different chlorite types illustrates a decrease of average temperature values (Figs. 10C, 12) accompanied by an increase of Mn contents firstly from early to late metamorphic chlorite associated with the metamorphic fabric (from parageneses 2 to 3), then up to late fluid circulation related chlo rite (paragenesis 4) overprinting earlier parageneses. Further, the average temperature estimate of ca. 310 ± 54 °C from chlorite associated with paragenesis 2 is consistent with greenschist grade conditions during regional metamorphism suggested for most parts of the Pongola Supergroup (Beukes and Cairncross, 1991; Hegner et al., 1984; Hunter and Wilson, 1988). Considering these temperature variations (Figs. 10C, 12), two scenarios may be proposed for the thermal history experienced by the Mozaan Group and for the associated mineral transformation processes: (1) retrograde metamorphism involving fluid circulations, or (2) hydrothermal alter-

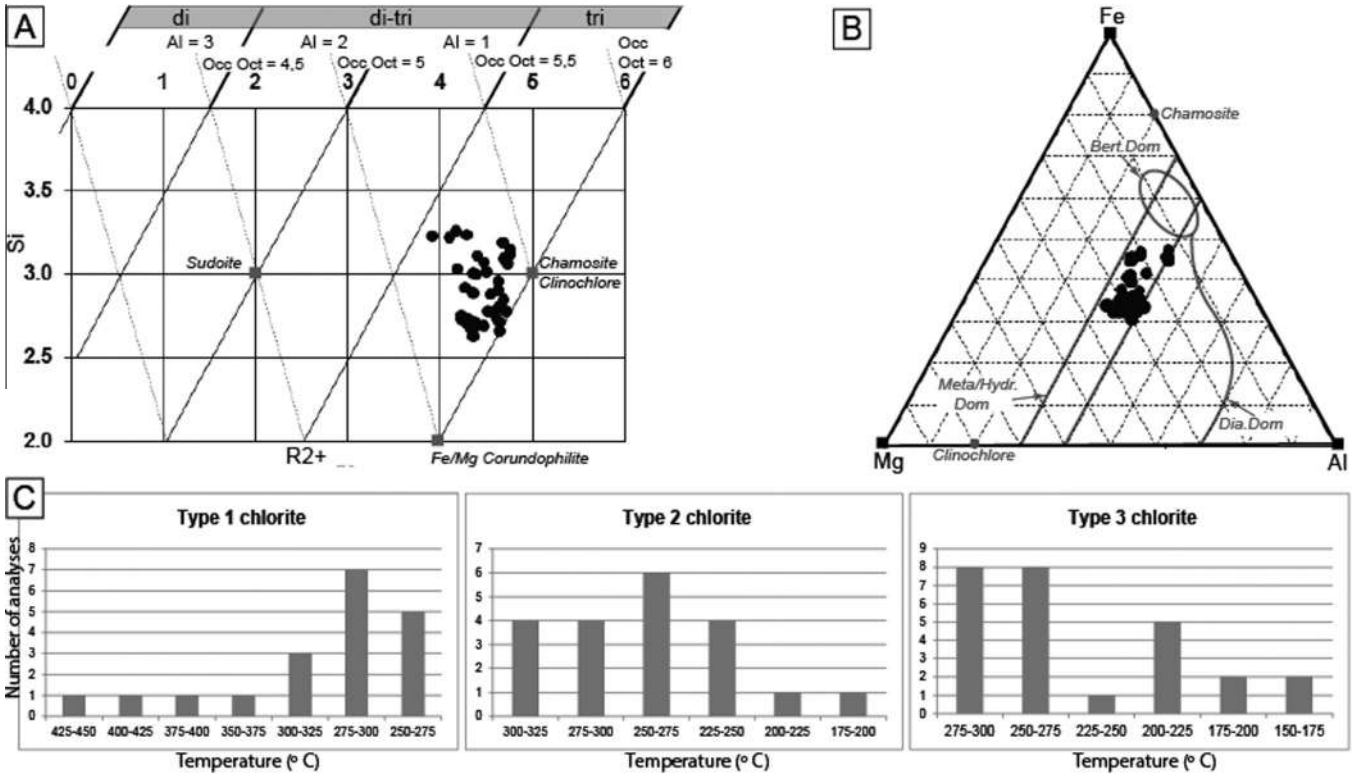

Fig. 10. Chlorite chemistry and thermometry. (A-B) Chemical composition of chlorite phases (based on 14 oxygen) plotted on A) diagram of vector representation of Wiewióra and Weiss (1990) and B) magnesium–aluminum-iron (Mg–Al–Fe) diagram (compositional fields after Velde, 1985); (C) Chlorite thermometry based on thermodynamic modeling from Vidal et al. (2005, 2006). (Bert.Dom: berthierine domain; Meta/Hydr.Dom: metamorphic/hydrothermal domain; Dia.Dom: diagenetic domain).

ation post dating greenschist facies metamorphism. The described thermal evolution and associated processes would have allowed a progressive enrichment of Mn, where MnO may reach about 15 wt. %, following local remobilization from early diagenesis to late hydrothermal alteration. Such processes, including diagenesis/ metamorphism and hydrothermal activity, are thought to have controlled mineral transformation as well as giving rise to Mn enrichment in some areas of the Giant Kalahri Mn deposits (Gutzmer and Beukes, 1995, 1997).

5.3. Timing of mineralization

$^{40}Ar/^{39}Ar$ dating was performed in order to estimate the timing of mineral transformation processes and related events. As K rich clay minerals are absent in unaltered rocks with parageneses 1 and 2, no dating was performed on these samples. However, K rich clay minerals were abundant in altered rock, where paragenesis 4 related to fluid circulation has overprinted earlier paragene ses, including 1, 2 and 3. $^{40}Ar/^{39}Ar$ dating performed on K rich phyllosilicate phases affected by fluid circulations (e.g. sample 93.1, 162.4, FR7 in Figs. 2 and 11) shows step dates ranging between 1500 and 1100 Ma, with high temperature integrated ages between 1490 and 1420 Ma.

The study area is situated approximately 60 km north of the contact with the Mesoproterozoic Namaqua Natal mobile belt, referred to as the Natal thrust front along which the Tugela terrane was thrust to the north (Thomas, 1989; Fig. 1). Elworthy et al. (2000) obtained Rb Sr biotite ages of 2614 ± 74 Ma for granitoids exposed more than 50 km north of the Natal Thrust Front and including those of the White Umfolozi Inlier, whereas Rb Sr biotite ages of ~933 990 Ma were found in localities within 25 km of the thrust front (e.g. Nkandla; Fig. 1). The authors regarded the older ages as cooling ages below the biotite closure temperature of 300 ° C following a late Archean regional metamorphic episode. A regional event at 2.72 Ga reaching up to granulite grade has been reported from the southeastern part of the Kaapvaal Craton (Hofmann et al., 2015). The younger Rb Sr biotite ages were ascribed to thermal overprinting during the Namaqua Natal orogeny (Elworthy et al., 2000). Although the dominant phase of deformation and peak metamorphism related to the Namaqua Natal orogeny occurred between 1.16 1.02 Ga, other Proterozoic events recorded at least in the Namaqua Natal Belt have been reported (Eglington, 2006). These include the formation of (1) juve nile crust within the Namaqua Natal Belt at about 1.4 Ga, (2) early juvenile mafic to intermediate igneous units formed between about 1.3 and 1.2 Ga, (3) igneous activity as part of the Namaqua Natal orogenesis, which was concluded by about 1.0 Ga throughout the belt (Eglington, 2006). In view of this, Ar Ar ages of c. 1430 Ma may hint to some Kalahari Craton margin processes that eventually led to Namaqua Natal belt evolution. Alternatively, these ages reflect Mesoproterozoic intraplate mag matism that gave rise to a series of alkaline and carbonatitic com plexes in the southern part of the Kalahari craton at ca. 1.4 1.35 Ga (Hanson et al., 2006), possibly also including the Bull's Run carbon atite complex situated just south of the Natal Thrust Front (Scogings and Forster, 1989).

The Ar Ar result of one sample of ca. 1110 Ma overlaps with ages of the main phase of Namaqua Natal orogeny between 1.16 and 1.02 Ga. Jacobs et al. (1997), using $^{40}Ar/^{39}Ar$ thermochronology, showed that thrusting within the Proterozoic Tugela Terrane, situated just south of the Natal Thrust Front (Fig. 1) occurred from ~1135 to 980 Ma. Furthermore, titanite fission track data of sam ples taken at regular intervals along a ~250 km traverse from the Natal Metamorphic front to the north into the Kaapvaal Craton

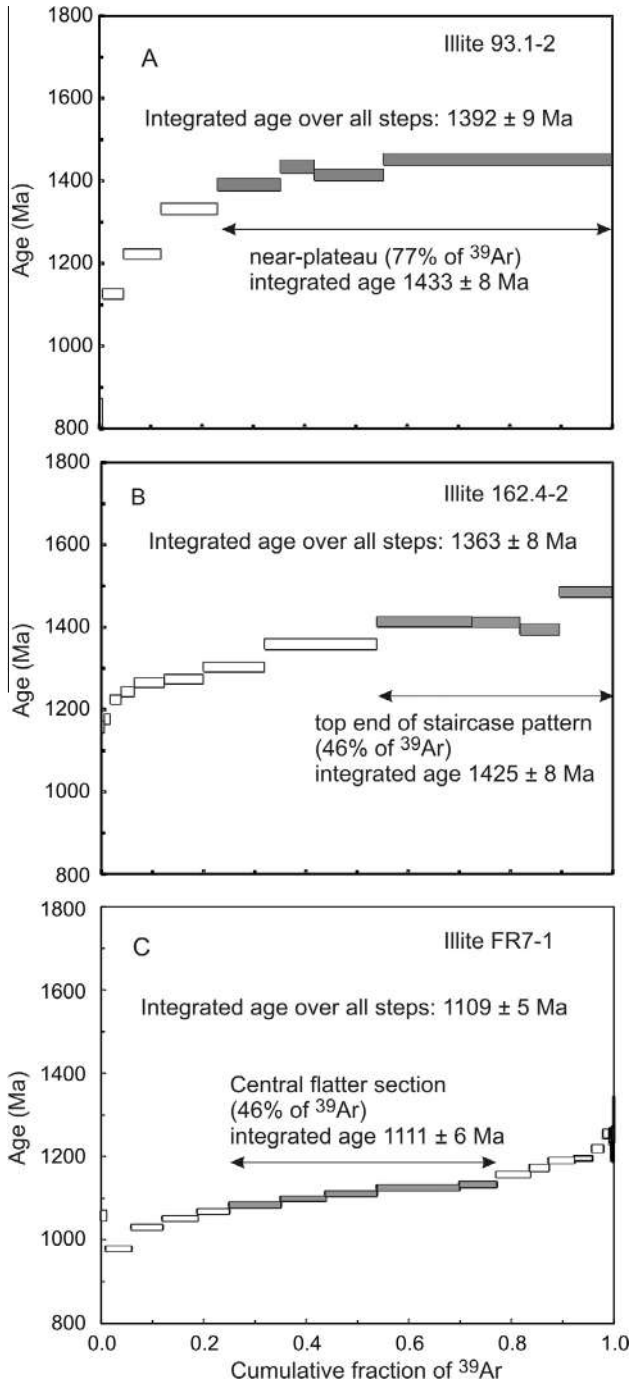

Fig. 11. Stepwise heating age spectra of aliquots of the <2 μm illite fraction from samples 162.4, 93.1 and FR7 (see Table S3 for step data). Error boxes reflect 95% confidence limits. Note general staircase nature of the patterns and broad consistency of the ages reflected by high temperature steps.

(Fig. 1) revealed a concentration of 1.1 Ga ages (Jacobs and Thomas, 2001). These ages were ascribed to cooling related to craton exhumation following tectonic loading of the crust by thrust sheets (Tugela nappes; Jacobs and Thomas, 2001). Therefore, our Ar Ar ages are interpreted to reflect a thermal overprint of the sedimentary rocks of the Pongola Supergroup in the White Mfolozi Inlier related to the formation of Namaqua Natal belt and, possibly, alkaline intraplate magmatism. Furthermore, the eastern part of the Kaapvaal Craton hosts several mafic dyke swarms dated at ca. 2.97 2.95, 2.87, 2.68 2.65, and 2.06 1.90 Ga (Klausen et al., 2010; Olsson et al., 2010; Gumsley et al., 2015), but also including mafic dykes and sills of the 180 Ma Karoo Igneous Province. These events may also had an effect on the rocks in the study area. In summary, a thermal event controlling mineral transformation processes and related hypogene Mn enrichment was an event unrelated to diagenesis in the Mesoarchean and probably also unrelated to metamorphism in the late Archean. Enrichment in manganese between 1.4 and 1.1 Ga ago in the study area thus took place at a similar time to Mn enrichment reported from the Kala hari-manganese field (Evans et al., 2001).

5.4. Mn Fe ore deposit potential of the Mozaan Group

The high Mn contents of the Mozaan Group could potentially be of economic interest. MnO contents up to 15 wt.% are unusual for the Mesoarchean record, where sedimentary Mn deposits are usually thought to be rather restricted (Maynard, 2010; Roy, 2000, 2006). Manganese iron deposits with such concentrations can be of economic significance. This is the case for the Woodstock iron manganese deposit in Canada that represents the largest Mn resource in North America with Mn contents up to 10% and associated Fe content as high as 13% (Potter, 1983; Sidwell, 1957). In this view, Mn rich ferruginous shale and BIF of the Mozaan Group potentially represent a Mn resource keeping in mind that the Pongola Supergroup crops out over a minimum depositional area of 32,500 km^2 (Button et al., 1981).

Except for a few examples described in the Giant Kalahari Mn field (Gutzmer and Beukes, 1997), almost all economically exploitable Mn or Mn Fe ores around the world have experienced supergene enrichment of low grade parent rocks into high grade ores (Roy, 2000, 2006). In the Francevillian Group of Gabon, for example, Paleoproterozoic carbonate protore initially characterized by Mn contents as high as 13% was mineralized up to about 45% by supergene processes (Gauthier Lafaye and Weber, 2003; Weber, 1997). High primary Mn contents could make the Mozaan Group a potential Mn or Mn Fe ore producer where affected by prolonged weathering episodes, such as below the African Surface that developed in the Late Cretaceous (Partridge, 1998). This warrants further investigations in the Mozaan Group where appreciable MnO contents have already been described. Limited previous exploration for Mn has indicated high grade Mn ores of up to 47% of Mn content in Mozaan shales in the Vryheid Piet Retief area and Bellevue, Northern KwaZulu Natal (De Villiers, 1960) indicating the potential for further investigations of the Mozaan Group. Such investigations could even be extended into other Mesoarchean sedimentary rocks of South Africa, such as the West Rand Group (including the Water Tower slates, Contorted Bed, Promise iron for mation), stratigraphically correlative with the Mozaan Group (Beukes and Cairncross, 1991), and where Mn contents up to 2% have been found in carbonate and Fe rich mudstone of the Promise Formation (Smith et al., 2013).

6. Conclusion

Rocks of the Mesoarchean Mozaan Group, Pongola Supergroup, in the White Mfolozi Inlier are characterized by MnO contents as high as 8.5 wt.% for unaltered rocks, whereas MnO contents may exceed 15 wt.% in altered rocks affected by fluid circulations. This variation in MnO contents is associated with mineral diversification and four different parageneses have been encountered. Their reconstruction has shown mineral transformation and evolution, from unaltered to altered rocks, from early diagenesis to metamorphism and late fluid circulation. These processes were associated with metal remobilization giving rise to progressive Mn enrichment from unaltered to altered rocks. Despite alteration, MnO contents as high as 8.53 wt.% reflect remarkably high rates

Type of paragenesis	Major minerals		Minor minerals		Temperature of formation (°C)	Thermal stage	Inferred age
	Phases	MnO (wt.%)	Phases	MnO (wt.%)			
Paragenesis 1	Fe-rds	30				Diagenesis	Mesoarchean
Paragenesis 2	Mn-sd Fe-chl	9 < 1	Kut Ank	18 5	310 ± 54	Metamorphism 1	Late Archean (Elworthy et al., 2000; Hofmann et al. 2015)
Paragenesis 3	Mn-Fe-chl Mn-sd Fe-teph Rds	2 17 30 51	Pyr Cstd	22 6	264 ± 34	Metamorphism 2	Mesoproterozoic (present study)
Paragenesis 4	Mn-Fe-chl Mn-sd Fe-teph Ca-rds Pcr Jcb	7 19 34 38 77 13	Ank Pyr Cstd Mn-phl	5 33 6 5	244 ± 41	Late fluid circulation	

Fig. 12. Synthesis of Mn-rich mineral parageneses and thermal events related to their occurrence.

of deposition of manganese rich sediment in shallow, Mesoarchean seawater. It appears that the precipitation of such an amount of Mn was directly controlled by an oxygenated tidally influenced shallow marine environment, thus representing a well preserved Mesoarchean oxygen oasis.

Thermodynamic modeling applied to chlorite phases of the different mineral parageneses shows a decrease of average values of crystallization temperatures: (1) from ca. 310 ± 54 (chlorite type 1) to 264 ± 34 °C (chlorite type 2), representing early to late stages of metamorphism; (2) ca. 244 ± 41 °C (chlorite type 3) associated with mineral phases related to late fluid circulations. Therefore, an event of retrograde metamorphism involving fluid circulations or hydrothermal alteration post dating metamorphism may have likely controlled local Mn remobilization and redistribution, accompanied by a progressive Mn enrichment in ferruginous shale and BIFs of the Mozaan Group. $^{40}Ar/^{39}Ar$ dating shows that hydrothermal type mineral transformation and associated Mn enrichment would have probably been a late and separate Meso proterozoic event, possibly related to the Namaqua Natal orogeny, rather than diagenesis or regional metamorphism in the Archean.

The Mozaan Group represents a unique example of Archean Mn enrichment, a more extensive investigation of which will allow for a better understanding of the nature, distribution and origin of sed imentary Mn deposition during the Archean in general, and in the Mozaan Group in particular. Moreover, further investigation will better define the potential and economic impact of Mn deposition within the Mozaan Group, across an area of about 32,500 km^2 of Pongola Supergroup exposure. Considering the first order control of redox conditions on manganese deposition, further sedimentary geochemistry and stable isotope studies of the Mn bearing Mesoarchean rocks of the Kaapvaal Craton will be helpful for better constraining the evolution and dynamics of Archean O_2 levels within the atmosphere ocean system, potentially enhancing our knowledge of the formation of mineral deposits associated with redox processes through time.

Acknowledgements

This study was funded by the National Research Foundation (NRF) of South Africa and the University of Johannesburg via a Post Doctoral Fellowship to FOO, a NRF research grant to AH and by the DST NRF Centre of Excellence for Integrated Mineral and Energy Resource Analysis (CIMERA). AH thanks Acclaim Explo ration NL, J. Hancox and N. Hicks for access to drill core samples. We would also like to thank the Editor for handling our manu script, as well as the Reviewer 1, the comments of whom have been highly relevant and useful.

Appendix A. Supplementary data

Supplementary data associated with this article can be found, in the online version, at http://dx.doi.org/10.1016/j.precamres.2016.06.009.

References

Alexander, B.W., Bau, M., Andersson, P., Dulski, P., 2008. Continentally-derived solutes in shallow Archean seawater: rare earth element and Nd isotope evidence in iron formation from the 2.9 Ga Pongola Supergroup, South Africa. Geochim. Cosmochim. Acta 72, 378–394.

Anbar, A.D., Holland, H.D., 1992. The photochemistry of manganese and the origin of banded iron formations. Geochim. Cosmochim. Acta 56, 2595–2603.

Bajoumy, H.M., Khedr, M.Z., Ahmed, A.H., 2012. Mineralogy, geochemistry and origin of Mn in the high-Mn iron ores, Bahariya Oasis, Egypt. Ore Geol. Rev. http://dx.doi.org/10.1016/j.oregeorev.2012.12.009.

Bekker, A., Holland, H.D., Wang, P.-L., Rumble III, D., Stein, H.J., Hannah, J.L., Coatzee, L.L., Beukes, N.J., 2004. Dating the rise of atmospheric oxygen. Nature 427, 117–120.

Beukes, N.J., 1973. Precambrian iron-formation in South Africa. Econ. Geol. 68, 960–1004.

Beukes, N.J., Cairncross, B., 1991. A lithostratigraphic-sedimentological reference profile for the late Archaean Mozaan Group, Pongola Sequence: application to sequence stratigraphy and correlation with the Witwatersrand Supergroup. S. Afr. J. Geol. 94, 44–69.

Beukes, N.J., Gutzmer, J., 1996. A voleanic-exhalative origin for the world's largest (Kalahari) manganese field. A discussion of the paper by D.H. Cornell and S.S. Schütte. Mineraleum Deposita 31, 242–245.

Beukes, N.J., Klein, C., 1990. Geochemistry and sedimentology of a facies transition from microbanded to granular iron-formation – in the early Proterozoic Transvaal Supergroup, South Africa. Precambr. Res. 47, 99–139.

Beukes, N.J., Lowe, D.R., 1989. Environmental control on diverse stromatolite morphologies in the 3000 Myr Pongola Supergroup, South Africa. Sedimentology 36, 383–397.

Beukes, N.J., Klein, C., Kaufman, A.J., Hayes, J.M., 1990. Carbonate petrography, kerogen distribution, and carbon and oxygen isotope variations in an early Proterozoic transition from limestone to iron-formation deposition, Transvaal Supergroup, South Africa. Econ. Geol. 85, 663–690.

Burke, K., Kidd, W.S.F., Kusky, T.M., 1985. The Pongola structure of southeastern Africa: the world's oldest preserved rift? J. Geodyn. 2, 35–49.

Button, A., Pretorius, D.A., Jansen, H., Stocklmayer, V., Hunter, D.R., Wilson, J.F., Wilson, A.H., Vermaak, C.A., Lee, C.A., Stagman, J.G., 1981. The cratonic environment: the Pongola Supergroup. In: Hunter, D.R. (Ed.), Precambrian of the Southern Hemisphere. Elsevier Scientific Publications Co., Amsterdam, pp. 501–510.

Canfield, D.E., 2005. The early history of atmospheric oxygen: homage to Robert M. Garrels. Annu. Rev. Earth Planet. Sci. 33, 1–36.

Crowe, S.A., Døssing, L.N., Beukes, N.J., Bau, M., Kruger, S.J., Frei Canfield, D.E., 2013. Atmospheric oxygenation three billion years ago. Nature 501, 535–538.

De Villiers, J., 1960. The manganese deposits of the Union of South Africa. Pretoria. Geol. Surv. S. Afr. Handb. 2, 263.

Delvigne, C., Cardinal, D., Hofmann, A., André, L., 2012. Stratigraphic changes of Ge/Si, REE+Y and silicon isotopes as insights into the deposition of a Mesoarchean banded iron formation. Earth Planet. Sci. Lett. 355–356, 109–118.

Dong, H., Hall, C.M., Peacor, D.R., Halliday, A.N., 1995. Mechanisms of argon retention in clays revealed by laser ^{40}Ar–^{39}Ar dating. Science 267, 355–359. Dong, H., Hall, C.M., Halliday, A.N., Peacor, D.R., Merriman, R.J., Roberts, B., 1997. $^{40}Ar/^{39}Ar$ illite dating of late Caledonian (Acadian) metamorphism and cooling of K-bentonites and slates from the Welsh Basin, U.K. Earth Planet. Sci. Lett. 150, 337–351.

Eglington, M.B., 2006. Evolution of the Namaqua-Natal Belt, Southern Africa – a geochronological and isotope geochemical review. J. Afr. Earth Sci. 46, 93–111.

Elworthy, T., Eglington, B.M., Armstrong, R.A., Moyes, A.B., 2000. Rb–Sr isotope constraints on the timing of late to post-Archaean tectonometamorphism affecting the southeastern Kaapvaal Craton. J. Afr. Earth Sci. 30, 641–650.

Evans, D.A.D., Gutzmer, J., Beukes, N.J., Kirschvink, J.L., 2001. Paleomagnetic constraints on ages of mineralization in the Kalahari manganese field, South Africa. Econ. Geol. 96, 621–631.

Gauthier-Lafaye, F., Weber, F., 2003. Natural nuclear fission reactors: time constraints for occurrence, and their relation to uranium and manganese deposits and to the evolution of the atmosphere. Precambr. Res. 120, 81–100.

Gold, D.J.C., 2006. The Pongola Supergroup. In: Johnson, M.R., Anhaeusser, C.R., Thomas, R.J. (Eds.), The Geology of South Africa. Geological Society of South Africa, Johannesburg/Council of Geoscience, Pretoria, pp. 135–148.

Gumsley, A., Olsson, J., Söderlund, U., de Kock, M., Hofmann, A., Klausen, M., 2015. Precise U–Pb baddeleyite age dating of the Usushwana Complex, southern Africa-Implications for the Mesoarchean magmatic and sedimentological evolution of the Pongola Supergroup, Kaapvaal Craton. Precambr. Res. 267, 174–185.

Gutzmer, J., Beukes, N.J., 1995. Fault-Controlled metasomatic alteration of Early Proterozoic sedimentary manganese ores in the Kalahari manganese field, South Africa. Econ. Geol. 90, 823–844.

Gutzmer, J., Beukes, N.J., 1997. Mineralogy and mineral chemistry of oxide facies manganese ores of the Postmasburg manganese field, South Africa. Mineral. Mag. 61, 213–231.

Gutzmer, J., Nhleko, N., Beukes, N.J., Pickard, A., Barley, M.E., 1999. Geochemistry and ion microprobe (SHRIMP) age of a quartz porphyry sill in the Mozaan Group of the Pongola Supergroup: implications for the Pongola and Witwatersrand Supergroups. S. Afr. J. Geol. 102, 139–146.

Gutzmer, J., Chisonga, B.C., Beukes, N.J., Mukhopadhyay, J., 2008. The geochemistry of Banded Iron Formation-hosted high-grade hematite-martite ores. Econ. Geol. 15, 157–183.

Hanson, R.E., Harmer, R.E., Blenkinsop, T.G., Bullen, D.S., Dalziel, I.W.D., Gose, W.A., Ward, S.E., 2006. Mesoproterozoic intraplate magmatism in the Kalahari Craton: a review. J. Afr. Earth Sci. 46, 141–167.

Hegner, E., Kröner, A., Hofmann, A.W., 1984. Age and isotope geochemistry of the Archaean Pongola and Usushwana suites in Swaziland, southern Africa: a case for crustal contamination of mantle-derived magma. Earth Planet. Sci. Lett. 70, 267–279.

Hegner, E., Kröner, A., Hunt, P., 1994. A precise U–Pb zircon age for the Archaean Pongola Supergroup Volcanics in Swaziland. J. Afr. Earth Sci. 18, 339–341.

Hicks, N., Hofmann, A., 2012. Stratigraphy and Provenance of the auriferous-uraniferous, fluvial to shallow-Marine Sinqeni Formation, Mozaan Group, Northern KwaZulu-Natal, South Africa. S. Afr. J. Geol. 115, 327–344. Hofmann, A., Kröner, A., Xie, H., Hegner, E., Belyanin, G., Kramers, J., Bolhar, R., Slabunov, A., Reinhardt, J., Horváth, P., 2015. The Nhlangano gneiss dome in south-west Swaziland – a record of crustal destabilization of the eastern Kaapvaal craton in the Neoarchaean. Precambr. Res. 258, 109–132.

Holland, H.D., 2002. Volcanic gases, black smokers, and the Great Oxidation Event. Geochim. Cosmochim. Acta 66, 3811–3826.

Holland, H.D., 2005. 100th anniversary special paper: sedimentary mineral deposits and the evolution of Earth's nearsurface environments. Econ. Geol. 100, 1489–1509.

Huneke, J.C., Smith, S.P., 1976. The realities of recoil; ^{39}Ar recoil out of small grains and anomalous age patterns in ^{39}Ar-^{40}Ar dating. In: Proceedings of Lunar Science Conference 7th, vol. 2, pp. 1987–2008.

Hunter, D.R., Wilson, A.H., 1988. A continuous record of Archaean evolution from 3.5 Ga to 2.6 Ga in Swaziland and northern Natal. S. Afr. J. Geol. 91, 57–74.

Ingri, J., 1985. Geochemistry of ferromanganese concretions in Barents Sea. Mar. Geol. 67, 101–119.

Inoue, A., Meunier, A., Patrier-Mas, P., Rigault, C., Beaufort, D., Vieillard, P., 2009. Application of chemical geothermometry to low-temperature trioctahedral chlorites. Clays Clay Miner. 57, 371–382.

Isley, A.E., Abbott, D.H., 1999. Plume-related mafic volcanism and the deposition of banded iron formation. J. Phys. Res. 104, 15461–15477.

Jacobs, J., Thomas, R.J., 2001. A titanite fission track profile across the southeastern Archaean Kaapvaal Craton and the IVlesoproterozoic Natal Metamorphic Province, South Africa: evidence for differential cryptic Meso- to Neoproterozoic tectonism. J. Afr. Earth Sci. 33, 323–333.

Jacobs, J., Falter, M., Thomas, R.J., Kunz, J., Jeßberger, E.K., 1997. $^{40}Ar/^{39}Ar$ thermochronological constraints on the structural evolution of the Mesoproterozoic Natal Metamophic Province, SE Africa. Precambr. Res. 86, 71–92.

Johnson, J.E., Webb, S.M., Thomas, K., Ono, S., Kirschvink, J.L., Fischer, W.W., 2013. Manganese-oxidizing photosynthesis before the rise of cyanobacteria. PNAS. http://dx.doi.org/10.1073/pnas.1305530110.

Kasting, J.F., 1993. Earth's early atmosphere. Science 259, 920–926.

Klausen, M.B., Söderlund, U., Olsson, J.R., Ernst, R.E., Armoogam, M., Mkhize, S.W., Petzer, G., 2010. Petrological discrimination among Precambrian dyke swarms: Eastern Kaapvaal craton (South Africa). Precambr. Res. 183, 501–522.

Konhauser, K.O., Hamade, T., Raiswell, R., Morris, R.C., Ferris, F.G., Southam, G., Canfield, D.E., 2002. Could bacteria have formed the Precambrian banded iron formations? Geology 30, 1079–1082.

Lepp, H., 2008. The relation of iron and manganese in sedimentary iron formations. Econ. Geol. 58, 515–526.

Lucchetti, G., 1991. Tephroite from the Val Graveglia metacherts (Liguria, Italy): mineral data and reactions for Mn-silicates and Mn-Ca-carbonates. Eur. J. Mineral. 3, 63–68.

Matthews, P.E., 1967. The pre-Karoo formations of the White Umfolozi inlier, northern Natal. Trans. Geol. Soc. South Afr. 70, 39–63.

Maynard, J.B., 2010. The chemistry of manganese ores through time: a signal of increasing diversity of earth-surface environments. Econ. Geol. 105, 535–552.

McDougall, M., Harrison, T.M., 1999. Geochronology and Thermochronology by the $^{39}Ar/^{40}Ar$ Method. Oxford University Press, p. 269.

Mossman, D.J., Pawson, D.J., 1976. X-ray and optical characterization of the fayalite-forsterite-tephroite series and comments on knebelite from Bluebell mine, British Columbia. Can. Mineral. 14, 479–486.

Nhleko, N., 2003. The Pongola Supergroup of Swaziland. PhD thesis of Rand Afrikaans University, p. 299.

Noffke, N., Hazen, R., Nhleko, N., 2003. Earth's earliest microbial mats in a siliciclastic marine environment (2.9 Ga Mozaan Group, South Africa). Geology 31, 673–676.

Noffke, N., Beukes, N., Bower, D., Hazen, R.M., Swift, D.J.P., 2008. An actualistic perspective into Archean worlds-(cyano-) bacterially induced sedimentary structures in the siliciclastic Nhlazatse Section, 2.9 Ga Pongola Supergroup. South Afr. Geobiol. 6, 5–20.

Olsson, J.R., Söderlund, U., Klausen, M.B., Ernst, R.E., 2010. U–Pb baddeleyite ages linking major Archean dyke swarms to volcanic-rift forming events in the Kaapvaal craton (South Africa), and a precise age for the Bushveld Complex. Precambr. Res. 183, 490–500.

Öztürk, H., 1997. Manganese deposits in Turkey: distribution, types and tectonic setting. Ore Geol. Rev. 12, 187–203.

Pack, A., Gutzmer, J., Beukes, N.J., Van Niekerk, H.S., 2000. Supergene ferromanganese wad deposits derived from Permian Karoo Strata along the late cretaceous–mid-tertiary African Land Surface, Ryedale, South Africa. Econ. Geol. 95, 203–220.

Partridge, T.C., 1998. Of diamonds, dinosaurs and diastrophism: 150 million years of landscape evolution in southern Africa. S. Afr. J. Geol. 101, 167–184.

Planavsky, N.J., Asael, D., Hofmann, A., Reinhard, C.T., Lalonde, S.V., Knudsen, A., Wang, X., Ossa Ossa, F., Pecoits, E., Smith, A.J.B., Beukes, N.J., Bekker, A., Johnson, T.M., Konhauser, K.O., Lyons, T.W., Rouxel, O., 2014. Evidence for oxygenic photosynthesis half a billion years before the Great Oxidation Event. Nat. Geosci. 7, 283–286.

Potter, R.R., 1983. The Woodstock iron works Carleton County, New Brunswick. CIM Bull. 76, 81–83.

Roy, S., 2000. Late Archean initiation of manganese metallogenesis: its significance and environmental controls. Ore Geol. Rev. 17, 179–198.

Roy, S., 2006. Sedimentary manganese metallogenesis in response to the evolution of the Earth system. Earth Sci. Rev. 77, 273–305.

Scogings, A.J., Forster, I.F., 1989. Gneissose carbonatites in the Bull's Run Complex, Natal. S. Afr. J. Geol. 92, 1–10.

Siahi, M., Hofmann, A., Hegner, E., Master, S., 2016. Sedimentology and facies analysis of Mesoarchean carbonate rocks of the Pongola Supergroup, South Africa. Precambr. Res. 278, 244–264.

Sidwell, K.O.J., 1957. The Woodstock, N.B., iron-manganese deposits. Trans. Can. Inst. Min. Metall. 50, 411–416.

Smith, A.J.B., Beukes, N.J., Gutzmer, J., 2013. The composition and depositional environments of Mesoarchean Iron Formations of the West Rand Group of the Witwatersrand Supergroup, South Africa. Econ. Geol. 108, 111–134.

Thomas, R.J., 1989. A tale of two tectonic terranes. South Afr. J. Geol. 92, 306–321.

Tsikos, H., Beukes, N.J., Moore, J.M., Harris, C., 2003. Deposition, diagenesis, and secondary enrichment of metals in the Palaeoproterozoic Hotazel Iron Formation, Kalahari manganese field, South Africa. Econ. Geol. 98, 1449–1462. Tsikos, H., Matthews, A., Erel, Y., Moore, J.M., 2010. Iron isotopes constrain biogeochemical redox cycling of iron and manganese in a Palaeoproterozoic stratified basin. Earth Planet. Sci. Lett. 298, 125–134.

Veizer, J., 1978. Secular variations in the composition of sedimentary carbonate rocks., II. Fe, Mn, Ca, Mg, Si and minor constituents. Precambr. Res. 6, 381–413.

Veizer, J., Garrett, D.E., 1978. Secular variations in the composition of sedimentary carbonate rocks, I. Alkali metals. In: Precambr. Res. 6, 367–380.

Velde, B., 1985. Clay Minerals a Physico-Chemical Explanation of Their Occurrence. Elsevier, Amsterdam.

Vidal, O., Parra, T., Vieillard, P., 2005. Thermodynamic properties of the Tschermak solid solution in Fe-chlorite: application to natural examples and possible role of oxidation. Am. Mineral. 90, 347–358.

Vidal, O., De Andrade, V., Lewin, E., Munoz, M., Parra, T., Pascarelli, S., 2006. P-T-deformation-Fe^{3+}/Fe^{2+} mapping at the thin section scale and comparison with XANES mapping: application to a garnet-bearing metapelite from the Sambagawa metamorphic belt (Japan). J. Metamorph. Geol. 24, 669–683.

Villa, I.M., 1997. Direct determination of ^{39}Ar recoil range. Geochim. Cosmochim. Acta 61, 689–691.
Von Brunn, V., Hobday, D.K., 1976. Early Precambrian tidal sedimentation in the Pongola Supergroup of South Africa. J. Sediment. Res. 46, 670–679.
Walshe, J.L., 1986. A 6-component chlorite solid-solution model and the conditions of chlorite formation in hydrothermal and geothermal systems. Econ. Geol. 81, 681–703.
Weber, F., 1997. Evolution of lateritic manganese deposits; in Soils and Sediments. In: Paquet, H., Clauer, N. (Eds.), Mineralogy and Geochemistry. Springer, p. 369.
Wiewiora, A., Weiss, Z., 1990. Crystallochemical classifications of phyllosilicates based on the unified system of projection of chemical composition: III. The chlorite group. Clay Miner. 25, 83–92.
Wronkiewicz, D.J., Condie, K.C., 1989. Geochemistry and provenance of sediments from the Pongola Supergroup, South Africa; evidence for a 3.0-Ga-old continental craton. Geochim. Cosmochim. Acta 53, 1537–1549.
Zaitsev, A.N., 1996. Rhombohedral carbonates from carbonatite of the Khibina Massif, Kola Peninsula, Russia. Can. Mineral. 34, 453–468.